Real-Time Localization Based on MIMO Backscattering From Retro-Directive Antenna Arrays

Marina Lotti, *Graduate Student Member, IEEE*, Nicolò Decarli, *Member, IEEE*, Gianni Pasolini, *Member, IEEE*, and Davide Dardari, *Fellow, IEEE*

***Abstract*—Precise localization is essential for enabling advanced applications in dynamic environments, such as autonomous systems and mobile robotics. As automation technologies evolve, the requirements for higher accuracy, reliability, energy efficiency, rapid updates, and minimal latency in position estimation have intensified. In this paper, we propose the exploitation of backscattering from retro-directive antenna arrays (RAAs) to address these imperatives. Two RAA-based architectures are introduced and evaluated for a range of applications, including network localization and navigation. These architectures enable swift and simple angle-of-arrival estimation by using signals backscattered from RAAs. They also leverage multiple antennas to capitalize on multiple-input-multiple-output (MIMO) gains, thereby addressing the challenges posed by the inherent path loss in backscatter communication, particularly at high frequencies. This approach enables angle-based localization with remarkably low latency, making it suitable for vehicular applications. To achieve this, ad-hoc signaling and processing schemes are developed and their performance is analytically assessed. Numerical results highlight the potential of these schemes, delivering precise, ultra-low-latency localization with low-complexity, energy-efficient devices.**

***Index Terms*—Localization, MIMO backscatter, positioning, retrodirectivity, retroreflection, self-conjugating metasurfaces.**

I. Introduction

TOWARD the realization of 6G, the integration of advanced localization and sensing capabilities holds paramount importance, enabling unprecedented levels of spatial awareness and context-driven intelligence to revolutionize communication, connectivity, and interaction in diverse domains [1], [2].

For instance, in vehicular networks, the integration of localization and sensing technologies is crucial for enhancing safety, efficiency, and connectivity by enabling real-time awareness of vehicle positions, and surrounding traffic dynamics [3], [4]. This becomes even more important when it comes to autonomous driving systems [5]: as the level of automation increases, so does the demand for enhanced accuracy, reliability, update rate, and reduced latency in position information delivery. In particular, position information must be updated several times per second (*high update rate*) to properly feed the control systems, and it must be extremely up-to-date (*extremely low latency*) to enable fast reactions even in high-speed contexts [6], [7], [8], [9]. Similar requirements also arise in various types of vehicular networks, including unmanned aerial vehicles (UAVs) [10] and those that involve mobile robots in industrial plants for optimizing operational efficiency and enhancing safety [11].

When localization demand comes together with stringent energy efficiency and low complexity requirements, radio backscattering represents a viable solution [12], [13], [14], [15]. Backscattering enables devices, namely tags, to transmit data through the reflection of interrogation signals [16]. This approach offers advantages such as ultra-low power consumption and low-complexity implementations since neither active transmitters nor complete radiofrequency (RF) chains are usually embedded in tags. Regrettably, the primary drawback of backscatter radio is the significant path loss, as the signal traverses the propagation channel twice. This results in a limited operating range, often just a few meters, as observed in radio frequency identification (RFID) applications [17]. Such constraints are exacerbated with higher frequencies (mmWave/THz) [18], making traditional backscatter schemes impractical for achieving high-accuracy localization.

A solution to counteract the path loss is the adoption of multiple-input multiple-output (MIMO) techniques, involving the integration of multiple antennas on both nodes engaged in the backscattering process (i.e., the emitter of the interrogation signal and the backscatter radio). However, this would require maintaining the respective beams aligned, which contradicts the low-complexity nature of backscatter radio, in which no channel state information (CSI) estimation can be performed.

Received 6 September 2024; revised 19 December 2024 and 7 February 2025; accepted 12 February 2025. Date of publication 18 February 2025; date of current version 18 July 2025. This work was supported in part by the European Union under the Italian National Recovery and Resilience Plan (NRRP) of NextGenerationEU, partnership on "Telecommunications of the Future" (PE00000001 - Program "RESTART"), in part by the National Recovery and Resilience Plan (NRRP), Mission 04 Component 2 Investment 1.5 – NextGenerationEU, Call for tender n. 3277 dated 30/12/2021, Award 0001052 dated 23/06/2022, and in part by the EU HORIZON-JU-SNS-2022 project TIMES under Grant 101096307. The review of this article was coordinated by Dr. Hongliang Zhang. *(Corresponding author: Marina Lotti.)*

Marina Lotti, Gianni Pasolini, and Davide Dardari are with the Dipartimento di Ingegneria dell'Energia Elettrica e dell'Informazione "Guglielmo Marconi" (DEI), University of Bologna, 40126 Bologna, Italy, and also with the WiLab-CNIT, 40133 Bologna, Italy (e-mail: marina.lotti2@unibo.it; gianni.pasolini@unibo.it; davide.dardari@unibo.it).

Nicolò Decarli is with the National Research Council - Institute of Electronics, Computer and Telecommunication Engineering (CNR-IEIIT), 10129 Torino, Italy, and also with WiLab-CNIT, 40133 Bologna, Italy (e-mail: nicolo.decarli@cnr.it).

Digital Object Identifier 10.1109/TVT.2025.3543140

In dynamic scenarios involving terrestrial vehicles or UAVs, beam alignment challenges are significantly heightened by the movement of objects, particularly at mmWave and THz frequencies due to the highly directional, pencil-like beams inherent to these bands [19]. Consequently, adopting backscatter-based devices with multiple antennas at high frequencies necessitates the development of innovative beamforming strategies. These strategies must dynamically adapt to the movement of communicating devices, minimize processing capabilities, and ideally maintain lower complexity compared to traditional beamforming approaches.

In this regard, retro-directive antenna arrays (RAAs) [20], [21] deserve special consideration. These arrays possess a unique property called *retrodirectivity*, enabling them to act as intelligent mirrors that reflect incoming signals back to the source's direction, without requiring explicit knowledge of the source's location [22]. This allows for efficient exploitation of the MIMO gain, even in backscatter radio solutions. It is worth noticing that retrodirectivity (also known as *retroreflection*) can also be obtained using the recently introduced reconfigurable intelligent surface (RIS) technology. However, this requires the knowledge of the source's position to properly configure the RIS phase-profile [23].

Actually, RAAs have undergone research attention across diverse applications, encompassing satellite communications [24], [25], and terrestrial communication systems [26]. However, only a few works considered RAAs for localization purposes, as for example [27]. In this work, the authors present a tag designed to achieve long-range capabilities by strategically reflecting incident waves back toward the reader. They leverage the large bandwidth offered by mmWave frequencies to enhance accuracy and propose to combine Fast Fourier Transform (FFT) based techniques and MUSIC algorithms for estimating angles and distances. The detection capability of a backscattering RAA-based RFID system is instead investigated in [28]. Here, the authors introduce an energy-autonomous, long-range-compatible RFID system operating at mmWave frequencies. Additionally, they present the results of experiments conducted to evaluate the device's performance and measure its detection range, showing a range of 80 meters. In [29] a radar system exploiting an RAA is shown. Initially emitting omnidirectional pulses, it gradually gains directivity toward the target, improving signal quality over successive pulses. In [30], an RAA is introduced that receives a 40 GHz navigation signal and accurately re-transmits a 120 GHz beam in the direction of the incoming wave, utilizing internal local oscillators. The authors present simulation results indicating that this antenna can track the incoming wave with a low relative error.

Previous studies have primarily focused on the enabling technologies and implementation aspects of RAAs, without systematically exploring their potential in localization networks, particularly in addressing the diverse requirements of various applications and signal processing challenges. Furthermore, to the best of the authors' knowledge, there remains a lack of ad-hoc, low-complexity processing schemes that can achieve optimal communication and localization performance in MIMO architectures utilizing backscattering RAAs, especially in mmWave/THz scenarios.

In this study, we explore the use of RAAs for localization networks involving mobile agents such as terrestrial vehicles, UAVs, and mobile robots operating in industrial environments. Specifically, we illustrate two strategies for enabling angle-based localization by leveraging RAAs and narrowband signals. The first strategy is suitable for network localization, where RAA-equipped mobile nodes are localized by a central localization engine. The second strategy involves fixed RAA-equipped devices deployed in the environment, which mobile nodes utilize for self-localization in navigation applications. Thus, we present an innovative real time locating system (RTLS) architecture that leverages MIMO ultra-low-energy backscattering from RAAs. Unlike traditional time-based localization methods relying on wideband signals, from example ultrawide bandwidth (UWB)-RTLS, this approach attains precise angle-based localization using narrowband signals and massive arrays.

To achieve this, we propose an iterative technique for automatic beam alignment between a multi-antenna transmitting node and an RAA. This enables rapid and straightforward angle-of-arrival (AoA) estimation, with optimal MIMO gain, enhancing both communication and estimation quality. By combining multiple AoA estimates obtained using RAAs, localization is finally achieved with significantly lower latency and higher update rates compared to current RTLS systems.

Our key contributions are as follows:

- We present two narrowband, angle-based, localization architectures leveraging RAAs in MIMO mobile wireless networks. The first architecture enables anchors (i.e., reference nodes) to localize user equipments (UEs) (Architecture 1: network localization), while the second allows UEs to localize themselves by utilizing anchors (Architecture 2: navigation).
- We propose a blind iterative scheme that realizes optimal beamforming and AoA estimation with extremely low latency. This is accomplished without requiring complex or explicit CSI estimation or beam alignment, and with no computational burden on the RAA side, ensuring minimal power consumption and simple hardware requirements for anchors and UEs.
- We describe how to handle multiple nodes, including multiple RAAs. According to the method proposed, frame-level synchronization with RAAs is not required, which eliminates the need for dedicated signaling and significantly reduces system complexity.
- We analytically and numerically evaluate the performance of the proposed localization strategies and introduce an ad-hoc solution to further reduce latency in dynamic scenarios. This ensures the system maintains high accuracy and responsiveness even in the presence of node mobility.

The rest of the paper is organized as follows. In Section II, we provide the fundamental concepts of RAAs, introduce the envisioned network architectures, and discuss their key components. Moving forward, in Section III, we demonstrate how RAAs can be exploited to enable AoA estimation, and we present a scheme capable of both deriving AoAs and extracting data bits from the backscattered signal, also addressing the case of multiple users. In Section IV, we analytically investigate the convergence of the proposed scheme and discuss the benefits of introducing

tracking capabilities at the channel level. Finally, in Section V, we present the numerical results, highlighting the performance of our solution and the main implementation challenges.

Notations and Definitions: Boldface lower-case letters are vectors (e.g., $\mathbf{x}$), whereas boldface capital letters are matrices (e.g., $\mathbf{H}$). $\|\mathbf{x}\|$ represents the Euclidean norm of $\mathbf{x}$. $\mathbf{H}^*$, $\mathbf{H}^\top$ and $\mathbf{H}^\dagger$ indicate, respectively, the conjugate, the transpose and the conjugate transpose operators applied to $\mathbf{H}$. The notation $x \sim \mathcal{CN}(m, \sigma^2)$ indicates a complex circular symmetric Gaussian random variable (RV) with mean m and variance σ^2, whereas $\mathbf{x} \sim \mathcal{CN}(\mathbf{m}, \mathbf{C})$ denotes a complex Gaussian random vector with mean $\mathbf{m}$ and covariance matrix $\mathbf{C}$.

II. Localization Using Retro-Directive Antenna Arrays

In this section, we begin by introducing RAAs, highlighting their key features that enable effective AoA estimation and communication. Next, we explore potential architectures envisioned for their application in localization and navigation. Finally, we conclude by outlining the fundamental building blocks required for the successful implementation of the proposed RTLS.

A. Retro-Directive Antenna Arrays

An RAA is a particular type of antenna array that operates based on the backscattering principle. The distinctive characteristic of an RAA is that its backscattering direction corresponds to the direction of the impinging signal, also denoted as interrogation signal, which is thus retro-directed toward the transmitter (retrodirectivity property). This behavior can be obtained, for instance, by conjugating the phase of the received signal at each antenna element of the RAA [22], using passive structures such as Van Atta arrays [31], or self-conjugating metasurfaces [32], [33].

Remarkably, backscattering toward the transmitter is achieved without requiring the estimation of the AoA of the signal impinging on the RAA. Unlike conventional antenna arrays that rely on phase shifters, the RAA operates independently of such mechanisms. This approach ensures low complexity and eliminates the need for control signals between the transmitter and the device equipped with the RAA. Additionally, by leveraging the architecture proposed in [34], data can be embedded by the RAA in the backscattered signal (e.g., containing the device unique identifier (ID)), thus establishing a communication link between the RAA-equipped device and a device that incorporates both the transmitter of the interrogation signal and the receiver aimed at capturing the signal reflected by the RAA. Specifically, we assume that these transmitters/receivers are equipped with multiple antennas, therefore we refer to them as MIMO transceivers (MIMO TRXs).

Concluding this short introduction on RAAs, it is important to note that the localization of UEs is commonly achieved through the deployment of a set of reference nodes, referred to as *anchors*, positioned at fixed known locations. Anchors and UEs interact to estimate the characteristics of position-dependent signals, such as the AoA [35]. In the following, we will illustrate how RAAs can be exploited both at the UE and anchor sides, leading to different architectural solutions, each with their own set of advantages and disadvantages.

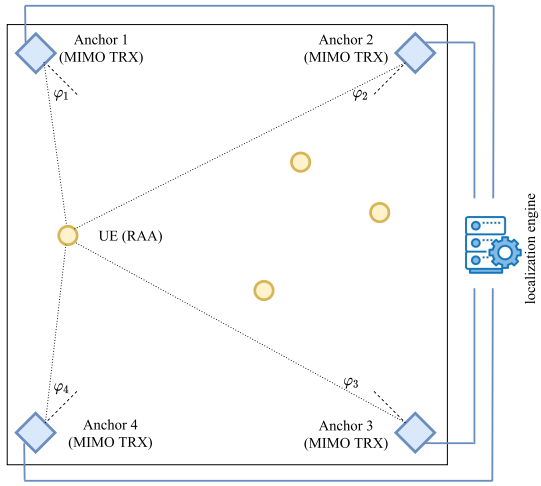

Fig. 1. Localization of RAAs-equipped mobile UEs (yellow circles) by using array-equipped anchors (blue squares). Anchors are also labelled a MIMO transceivers (TRX).

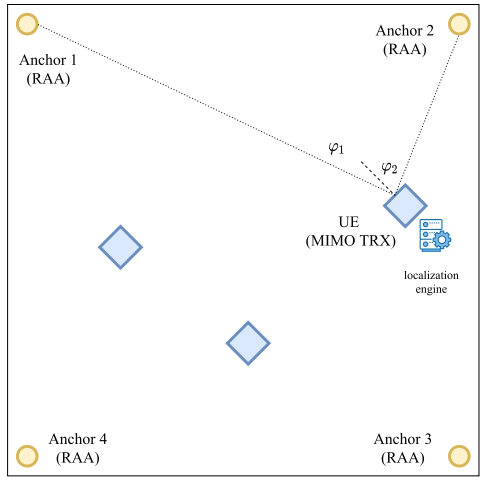

Fig. 2. Navigation of array-equipped mobile UEs (blue squares) through the interaction with RAAs (yellow circles) used as anchor nodes. UEs are also labelled MIMO transceivers (TRX).

B. Architectures

We designate *Architecture 1* as the configuration where RAAs are employed on mobile UEs, while anchor nodes use conventional antenna arrays (see Fig. 1), thus acting as MIMO TRXs. Conversely, *Architecture 2* involves RAAs for anchors while UEs are equipped with conventional antenna arrays, thus acting as MIMO TRXs (see Fig. 2). In vehicular contexts, for instance, RAAs could be used on board swarms of drones to be localized (*network localization* application). In contrast, RAAs could serve as reference nodes (anchors) for the self-localization of autonomous vehicles (*navigation* application). In the following, we introduce the fundamental building blocks necessary for realizing communication and AoA estimation by leveraging the availability of RAAs-equipped devices, either anchors or UEs, in the scenario.

1) Architecture 1 - RAA at the UE Side: Each mobile UE is equipped with an RAA (Fig. 1), while each anchor is equipped with a conventional array and is configured to transmit an interrogation signal, thus being a MIMO TRX. This signal is backscattered by the RAAs, which also embed their IDs, and subsequently received by the same anchor. The anchor can then estimate the AoAs of the signals received by the RAAs and extract their IDs using the scheme introduced in the Section III. Such information is then passed to a localization engine, which is in charge of estimating the UEs' positions based on the data received by all anchors. Specifically, once a sufficient number of AoA measurements are collected for a given RAA, the localization engine can localize the corresponding UEs, knowing the anchors' positions and orientations. For example, at least two AoAs per UE are needed for unambiguous 2D localization. Clearly, the larger the number of AoA measurements for each UE, the better will be the localization accuracy. To deal with measurement errors, the localization engine can fuse multiple AoAs estimates by leveraging, for instance, standard tools such as least squares or particle filtering.[1] Simultaneous access to UEs by different anchors can be achieved by exploiting distinct frequencies, assuming a flat frequency response of the RAA within the signal bandwidth. The discrimination of the backscatter components associated with different UEs, can be accomplished leveraging the spatial selectivity of the antenna array, as detailed in Section III-C.

This architecture is primarily tailored for network localization applications, allowing the network to comprehensively determine the positions of all UEs within the area of interest. It supports a wide range of use cases, including asset and personnel tracking, logistics management, and more. A key advantage of this architecture is the simplicity of the UEs, which require no processing capabilities. The UE merely backscatter the incoming signal via the RAA, embedding its ID into the reflected signal. This eliminates the need for complex RF chains or baseband components in the UEs, significantly reducing cost and complexity. Additionally, the architecture enables the use of energy harvesting techniques, allowing the UEs to operate autonomously with minimal power requirements.

2) Architecture 2 - RAA at the Anchor Side: This architecture entails equipping each anchor node with an RAA, while UEs utilize a conventional antenna array, thus being MIMO TRXs (Fig. 2). In contrast to Architecture 1, in this scenario, it is the anchor that responds to the interrogation signal emitted by the UE, leveraging retrodirectivity. Consequently, each UE must detect the presence of the RAA-equipped anchors, extracting their IDs, and estimate the AoAs of the retro-directed signals relative to its local coordinate system. A decentralized localization engine operates within each UE, enabling the estimation of its position.

This architecture is primarily tailored for navigation purposes, resembling GNSS-like positioning, as the position computation takes place at the UE. In this setup, localization information is immediately available to the UE, minimizing latency in scenarios where rapid position awareness is critical. This is particularly important when position data is required to feed control systems, such as in autonomous driving applications involving vehicles, UAVs, and mobile robots. In the context of vehicular networks, this architecture is particularly well-suited for the self-localization of autonomous vehicles, where onboard systems typically do not face complexity constraints. Simple, low-cost, and potentially energy-autonomous tags, equipped with RAAs and deployed throughout the environment, can serve as reference for navigation. This architecture can be further improved by enabling the RAA-based devices to transmit not only their ID but also their coordinates. This additional information allows the UE to perform localization without requiring prior knowledge of the anchors' deployment layout. Moreover, in a practical implementation, multiple anchors can be seamlessly integrated into the system without the need to update the anchor database on the UE side.

Different UEs can access simultaneously the RAA-based anchors by, for instance, utilizing different frequencies. As will be further clarified in Section III-C, a given UE can address simultaneously different anchors thanks to the spatial discrimination enabled by antenna arrays with a large number of elements and the scheme presented below.

Notice that, in Architecture 1, the AoA estimation is performed by anchor nodes that are aware of the absolute reference system. In contrast, in Architecture 2, the orientation of the UE may be unknown and must be estimated to determine the UE's absolute coordinates. In this case the UE localizes itself relative to its own local reference system rather than the absolute one. To map the result to an absolute reference system, the orientation of the UE must be known, either a priori or through additional sensors, such as an inertial sensor or a compass.

Remark: The proposed architectures enable the realization of a RTLS by leveraging angular measurements obtained through RAAs that operate with narrowband signals, offering improved spectrum usage efficiency. This method shifts the focus from the wide bandwidth typically used in UWB-based RTLSs to an increased number of antenna elements—an approach that is garnering significant attention, especially with the rise of metasurfaces. In traditional high-accuracy localization techniques, the time-of-arrival (TOA) or time difference-of-arrival (TDOA) of signals is estimated, with resolution tied to the bandwidth. Achieving centimeter-level accuracy typically requires around 1 GHz of bandwidth, which limits communication throughput when radio resources must be shared among communication and localization. Moreover, time-based methods are highly sensitive to clock mismatches between devices, making them less suitable for Internet-of-things (IoT) applications. Our approach, in contrast, allows for localization without relying on stringent synchronization or bandwidth-intensive low-efficient methods such as TOA-based two-way ranging. As a result, it reduces the complexity and cost of the infrastructure, overcoming a major obstacle to deploying high-accuracy positioning systems. Additionally, the backscatter nature of the scheme simplifies the devices and eliminates the issue of clock mismatches.

C. Building Blocks

To effectively implement the proposed architectures, specific building blocks and dedicated methods are required. It is important to note that in both architectures, MIMO TRXs are

[1]The reader can refer to [35].

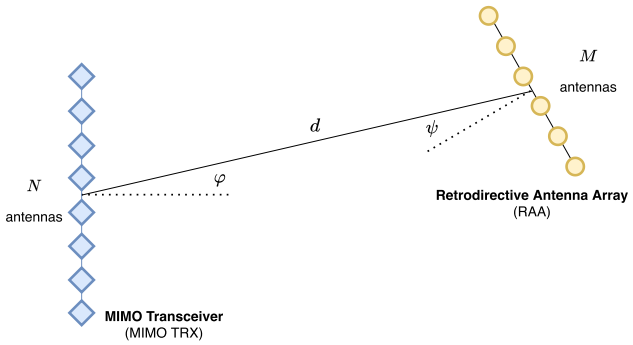

Fig. 3. Geometry of the scenario. MIMO TRX equipped with a N-antennas ULA; RAA composed of M antennas organized as ULA.

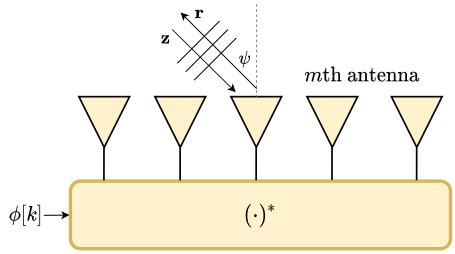

Fig. 4. Schematic representation of an RAA organized as ULA.

adopted. The use of multiple antennas is essential to counteract the unfavorable path loss typical of backscatter communication as well as to allow the estimation of the signal's AoA. Thus, the same antenna array can be used for transmission and reception by exploiting a full-duplex radio implementation, as is commonly done in monostatic radar applications [36].

The primary challenge in both architectures lies in determining the beamforming vector at the MIMO TRX to direct the interrogation signal toward the RAA, whose direction is unknown before AoA estimation. To address this challenge, we propose an iterative procedure inspired by [34], leveraging the distinctive capability of RAAs to reflect the signal in the same direction it was received. This approach allows for the automatic determination of the optimal beamforming vector at the transmitter's side without requiring explicit channel estimation and signaling. Remarkably, the process of determining the beamforming vector also yeld the AoA of the backscattered signal, which can then be used for localization. Since a MIMO link is finally established, the communication benefits from the MIMO gain to mitigate the high path loss. This procedure will be detailed in Section III.

III. AoA Estimation Based on RAAs

In this section, we outline a procedure for the MIMO TRX to estimate the AoA of the signal backscattered by an RAA using a blind iterative approach. This method guides the MIMO TRX to direct its interrogation signal toward the RAA. The procedure is then extended to support multiple RAA-based devices, allowing for simultaneous estimations.

A. System Model

We start by considering only two nodes, namely, a MIMO TRX and an RAA. The MIMO TRX is equipped with a uniform linear array (ULA) comprising N elements, capable of full-duplex communications. The RAA is realized as a uniform linear array consisting of M elements, without processing capabilities (refer to Fig. 3). Here, we focus on uniform linear arrays for simplicity of explanation, although various array layouts can be explored, as demonstrated in the numerical results. Both arrays are located in the far-field region of each other, separated by a distance d. The angle-of-departure (AoD) of the signal emitted by the MIMO TRX, when directed toward the RAA, is denoted as φ, while the AoA of the signal received at the RAA from the MIMO TRX is denoted as ψ.

The scheme we propose involves transmitting from the MIMO TRX to the RAA using a certain beamforming vector $\mathbf{x} \in \mathbb{C}^{N\times 1}$, ideally aligned with direction φ. Thanks to the retrodirectivity capability, the signal impinging the RAA is backscattered toward the direction of arrival (i.e., angle ψ). The backscattered signal is then received by the MIMO TRX by exploiting a full-duplex radio. This signal exchange, from the MIMO TRX to the RAA and back, takes place iteratively, once every T seconds corresponding to the symbol time. The time axis is thus segmented into intervals, indexed by k.

At the startup, the optimal beamforming vector is not known by the MIMO TRX, which therefore randomly generates a unit norm beamforming vector $\mathbf{x}[0]$. As will be detailed in Section III-B, at the end of each time interval k, with $k \geq 1$, the beamforming vector $\mathbf{x}[k]$ will be iteratively updated with a scheme allowing convergence toward the direction φ, finally establishing an optimal MIMO link between the two nodes.

Let $\sqrt{P_\mathrm{T}}\,\mathbf{x}[k] \in \mathbb{C}^{N\times 1}$ be the vector containing the signal transmitted by the N elements of the MIMO TRX's antenna array, where P_T is the transmitted power and $\mathbf{x}[k]$ is the unit norm beamforming vector at the generic time interval k. At the other end of the communication link, consider a plane wave impinging on the RAA, the schematic representation of which is shown in Fig. 4, with an angle ψ with respect to its normal direction. At the m-th RAA antenna, the impinging wave accumulates a phase shift θ_m, with respect to the first antenna, given by

$$\theta_m = \frac{2\pi}{\lambda} m\Delta \sin\psi \tag{1}$$

for $m = 0, 1, \ldots, M-1$, where Δ is the inter-antenna spacing and λ is the wavelength. By introducing the noise generated by the RAA, which is present in case it is implemented using active components [37], [38], the discrete-time signals at the input of the M antennas at the k-th time interval can be expressed by the vector

$$\mathbf{z}[k] = \alpha[k]\left[1,\, e^{\jmath\theta_1},\, \ldots,\, e^{\jmath\theta_{M-1}}\right]^\top + \boldsymbol{\eta}[k] \tag{2}$$

where $\alpha[k]$ is the signal at the first antenna, $\boldsymbol{\eta}[k] \in \mathbb{C}^{M\times 1}$ is the additive white Gaussian noise (AWGN), with $\boldsymbol{\eta}[k] \sim \mathcal{CN}(\mathbf{0}, \sigma_\eta^2 \mathbf{I}_M)$. Note that $\sigma_\eta^2 = \kappa T_0 F_\mathrm{RAA}\, W$, where κ represents the Boltzmann constant, $T_0 = 290\,\mathrm{K}$ denotes the reference temperature, F_RAA stands for the RAA's noise figure, and W indicates the signal bandwidth. Regarding the latter, we consider a narrowband transmission, such as a resource

block in an orthogonal frequency division multiplexing (OFDM) communication scheme.

To realize the retrodirectivity property, the phase profile of the reflected signal along the array must be opposite of that of the impinging signal. Therefore, the vector $\mathbf{r}[k]$ representing the signal backscattered by the RAA during the same time interval should be [22]

$$\mathbf{r}[k] = g\,\mathbf{z}^*[k] \tag{3}$$

where g is the gain of the RAA ($g < 1$ if passive).[2]

In addition to conjugating the received signal, we assume that the RAA introduces a phase shift $\phi[k]$ into the backscattered signal during the k-th time interval. This phase shift conveys information from the RAA to the MIMO TRX during that interval. For instance, this information could include a unique signature of the specific node, such as its ID. Note that the phase shift $\phi[k]$ is the same across all antennas, thereby preserving the retrodirectivity property. The vector representing the signal reflected by the RAA becomes therefore

$$\mathbf{r}[k] = g\,e^{\jmath\phi[k]}\,\mathbf{z}^*[k]\,. \tag{4}$$

By denoting the channel matrix between the MIMO TRX and the RAA with $\mathbf{H} \in \mathbb{C}^{M\times N}$, the signal received by the RAA at time instant k is given by

$$\mathbf{z}[k] = \sqrt{P_\mathrm{T}}\,\mathbf{H}\,\mathbf{x}[k-1] + \boldsymbol{\eta}[k] \tag{5}$$

and the retro-directed signal, according to (4), is

$$\mathbf{r}[k] = g\,e^{\jmath\phi[k]}\,\mathbf{z}^*[k] = \sqrt{P_\mathrm{T}} g e^{\jmath\phi[k]}\mathbf{H}^*\mathbf{x}^*[k-1] + g\boldsymbol{\eta}^*[k]\,. \tag{6}$$

Considering a free-space line-of-sight (LOS) scenario, and denoting with G_A and G_RAA the gain of each antenna element at the MIMO TRX and RAA, respectively, the channel matrix $\mathbf{H}$ takes the form

$$\begin{aligned}\mathbf{H}(\varphi,\psi) &= \sqrt{G_\mathrm{A}\,G_\mathrm{RAA}}\,\frac{\lambda}{4\pi d}\underbrace{\begin{bmatrix}1\\ e^{-\jmath\frac{2\pi}{\lambda}\Delta\sin\psi}\\ \vdots\\ e^{-\jmath\frac{2\pi}{\lambda}(M-1)\Delta\sin\psi}\end{bmatrix}}_{\tilde{\mathbf{u}}(\psi)\in\mathbb{C}^{M\times 1}}\\ &\quad\times\underbrace{\begin{bmatrix}1 & e^{-\jmath\frac{2\pi}{\lambda}\Delta\sin\varphi} & \dots & e^{-\jmath\frac{2\pi}{\lambda}(N-1)\Delta\sin\varphi}\end{bmatrix}}_{\tilde{\mathbf{v}}^\top(\varphi)\in\mathbb{C}^{1\times N}}\\ &= \sqrt{G_\mathrm{A}\,G_\mathrm{RAA}}\,\frac{\lambda}{4\pi d}\tilde{\mathbf{u}}(\psi)\tilde{\mathbf{v}}^\top(\varphi)\end{aligned} \tag{7}$$

where we have highlighted with $\mathbf{H}(\varphi,\psi)$ the dependence of the channel on the AoD φ at the MIMO TRX and AoA ψ at the RAA. It is worth noting that the channel matrix $\mathbf{H}(\varphi,\psi)$ depends on the angles φ and ψ (i.e., on the geometry of the scenario), regardless of whether the beamforming vector at the MIMO TRX's side $\mathbf{x}[k]$ corresponds to the beam steering vector in the direction φ (i.e., the optimal direction to convey power toward the RAA) or not.

By defining the vectors $\mathbf{u}(\psi) = \tilde{\mathbf{u}}(\psi)/\sqrt{M} \in \mathbb{C}^{M\times 1}$ and $\mathbf{v}(\varphi) = \tilde{\mathbf{v}}^*(\varphi)/\sqrt{N} \in \mathbb{C}^{N\times 1}$, it results

$$\mathbf{H}(\varphi,\psi) = \sqrt{NMG_\mathrm{A}\,G_\mathrm{RAA}}\,\frac{\lambda}{4\pi d}\mathbf{u}(\psi)\mathbf{v}^\dagger(\varphi) \tag{8}$$

which has rank one since obtained as an outer product of two vectors $\mathbf{u}$ and $\mathbf{v}^*$. Notice that $\mathbf{u}$ and $\mathbf{v}$ are, respectively, the top left and right eigenvectors of matrix $\mathbf{H}(\varphi,\psi)$ and hence give the optimal beamforming vectors at the RAA side and at the MIMO TRX.[3] We can introduce the singular-value decomposition (SVD) of $\mathbf{H}(\varphi,\psi)$ as $\mathbf{H}(\varphi,\psi) = \mathbf{U}\Sigma\mathbf{V}^\dagger$ where Σ has a singular non-zero entry

$$\sigma_1 = \frac{\sqrt{NMG_\mathrm{A}\,G_\mathrm{RAA}}\lambda}{4\pi d} \tag{9}$$

in its first element, $\mathbf{U}$ has $\mathbf{u}(\psi)$ as the first eigenvector (i.e., first column), and $\mathbf{V}$ has $\mathbf{v}(\varphi)$ as the first eigenvector (i.e., first column).

Assuming channel reciprocity, at the MIMO TRX side the received signal at time interval k, consisting of the feedback of the signal transmitted in the last time interval, is given by[4]

$$\begin{aligned}\mathbf{y}[k] = &\sqrt{P_\mathrm{T}}\,g\,e^{\jmath\phi[k]}\,\mathbf{H}^\top(\varphi,\psi)\,\mathbf{H}^*(\varphi,\psi)\,\mathbf{x}^*[k-1]\\ &+ g\,\mathbf{H}^\top(\varphi,\psi)\,\boldsymbol{\eta}^*[k] + \mathbf{w}[k]\end{aligned} \tag{10}$$

with $\mathbf{w}[k] \sim \mathcal{CN}(\mathbf{0}, \sigma_w^2\mathbf{I}_N)$ being the AWGN at the receiver, and $\sigma_w^2 = \kappa T_0 F_\mathrm{A}\,W$, where F_A represents the MIMO TRX's noise figure. By defining $\mathbf{A}(\varphi) = \sqrt{P_\mathrm{T}}\,g\,\mathbf{H}^\dagger(\varphi,\psi)\mathbf{H}(\varphi,\psi) \in \mathbb{C}^{N\times N}$, according to (8) it results

$$\mathbf{A}(\varphi) = \sqrt{P_\mathrm{T}}\,gNMG_\mathrm{A}G_\mathrm{RAA}\left(\frac{\lambda}{4\pi d}\right)^2\mathbf{v}(\varphi)\mathbf{v}^\dagger(\varphi) \tag{11}$$

which depends only on the angle φ, thanks to the retrodirectivity property of the RAA. Moreover, $\mathbf{A}$ is proportional to the (modified) round-trip channel $\mathbf{H}^\dagger(\varphi,\psi)\mathbf{H}(\varphi,\psi)$, rather than the (true) round-trip channel $\mathbf{H}^\top(\varphi,\psi)\mathbf{H}(\varphi,\psi)$ as in conventional backscatter communications. Consequently, the eigenvectors of $\mathbf{A}$ are identical to the right-eigenvectors of $\mathbf{H}(\varphi,\psi)$. From (10) we have

$$\mathbf{y}[k] = e^{\jmath\phi[k]}\,\mathbf{A}^*(\varphi)\,\mathbf{x}^*[k-1] + \mathbf{n}^*[k] \tag{12}$$

where we have defined $\mathbf{n}^*[k] = g\,\mathbf{H}^\top(\varphi,\psi)\,\boldsymbol{\eta}^*[k] + \mathbf{w}[k]$. Substituting (11) into (12) we obtain (13). In case of perfect beamforming, i.e., $\mathbf{x}[k-1] = \mathbf{v}(\varphi)$, the useful term $\tilde{\mathbf{y}}[k]$ in (13) shown at the bottom of the next page, becomes

$$\tilde{\mathbf{y}}[k] = \sqrt{P_\mathrm{T}}\,g\,e^{\jmath\phi[k]}MNG_\mathrm{A}G_\mathrm{RAA}\left(\frac{\lambda}{4\pi d}\right)^2\mathbf{v}^*(\varphi) \tag{14}$$

[2]From an implementation viewpoint, the conjugation in (3) can be obtained explicitly by means of an active circuit based on the superheterodyne principle [22], [39]. Alternatively, passive solutions can be adopted based on Van Atta arrays [40] or ad-hoc designed metasurfaces, which yield an equivalent result in the far-field region of the RAA [32], [33].

[3]Since $\mathbf{H}(\varphi,\psi)$ has rank one, $\mathbf{u}$ and $\mathbf{v}$ correspond to the only left and right eigenvectors associated with non-zero eigenvalues. In this sense, they are referred to as the top eigenvectors.

[4]For simplicity, in this model we do not consider clutter, that is, the signal backscattered by the environment and not modulated by the RAA. The reader can refer to [34] for a discussion concerning the modelling of the clutter and its impact on communication.

since $\mathbf{v}^\top \mathbf{v}^* = 1$, thus corresponding to a plane wave of power proportional to $P_\mathrm{T}\, M^2\, N^2/\mathcal{L}^2(d)$ impinging with AoA φ, where

$$\mathcal{L}(d) = \left(\frac{4\pi d}{\lambda}\right)^2 \tag{15}$$

is the link loss for a distance d in free space. Notice that due to the backscattering communication type, the path loss increases with the distance to the power of four, as happens in RFID systems [41]. On the other hand, thanks to the adoption of multiple antennas on both sides, such large path loss can be compensated by increasing the number of antenna elements N and M at the MIMO TRX and RAA, respectively (beamforming gain).

In the following section, we show how the beamforming vector $\mathbf{x}[k]$ at the MIMO TRX side can can be iteratively adjusted until it converges to the channel eigenvector $\mathbf{v}(\varphi)$ pointing toward the RAA. This process enables the desired property to be achieved without the need for explicit channel estimation. Thanks to the estimation of the optimal beamforming vector, the presence of the RAA can be detected, and the AoA of the backscattered signal is inherently obtained.

B. RAA Detection and AoA Estimation

The scheme we propose for RAA detection, identification, and AoA estimation operates iteratively. As shown in the associated pseudocode (Algorithm 1), to which the reader is referred, the process starts (step 1 of the pseudocode) with the generation of a random unitary beamforming vector $\mathbf{x}[0]$, which the MIMO TRX uses at startup when the locations of RAAs are still unknown.

The iterative procedure, which occurs with discrete time steps indexed by $k \geq 1$ (step 2), can then begin with the MIMO TRX transmitting the beamforming vector $\sqrt{P_\mathrm{T}}\,\mathbf{x}[k-1]$ (step 3). The RAA, upon receiving $\mathbf{z}[k] = \sqrt{P_\mathrm{T}}\mathbf{H}\mathbf{x}[k-1] + \boldsymbol{\eta}[k]$ (see (5)), backscatters it in the direction of arrival, as a result of the conjugation operation. Additionally, it introduces a phase modulation based on the data to be transmitted to the MIMO TRX, resulting in the reflected signal $\mathbf{r}[k] = g\, e^{\jmath\phi[k]}\mathbf{z}^*[k]$ (see (6)). The MIMO TRX then receives the retro-directed and modulated response $\mathbf{y}[k] = e^{\jmath\phi[k]}\, \mathbf{A}^*(\varphi)\, \mathbf{x}^*[k-1] + \mathbf{n}^*[k]$, as described by (12) (step 4).

At the MIMO TRX, a normalized and conjugated version of the received vector $\mathbf{y}[k]$ is computed (step 5) as $\mathbf{x}[k] = \frac{\mathbf{y}^*[k]}{\|\mathbf{y}[k]\|}$. This vector will be used as the updated beamforming vector $\mathbf{x}[k]$ in the next iteration. This adjustment makes the beamforming vector steer toward the RAA. In principle, the updated beamforming vector should immediately align with the RAA. However, due to the presence of noise and multipath, the alignment may require more than one iteration to be completed.

Algorithm 1: RAA Detection and AoA Estimation.

1: Generate a random unitary norm beamforming vector $\mathbf{x}[0]$
2: **for** $k = 1, 2, \ldots, \infty$ **do**
3: Transmit: $\sqrt{P_\mathrm{T}}\,\mathbf{x}[k-1]$
4: Receive: $\mathbf{y}[k] = e^{\jmath\phi[k]}\, \mathbf{A}^*(\varphi)\, \mathbf{x}^*[k-1] + \mathbf{n}^*[k]$
5: Update the beamforming vector: $\mathbf{x}[k] = \mathbf{y}^*[k]/\|\mathbf{y}[k]\|$
6: Create the decision variable: $u[k] = \mathbf{x}^\dagger[k-1]\,\mathbf{y}^*[k]$
7: Estimate the SNR: $\gamma[k] = |u[k]|^2/\sigma_w^2$
8: **if** $\gamma[k] > \eta_1$ and $\gamma[k]/\gamma[k-1] < \eta_2$ **then**
9: $\bar{k} = k$
10: DFT computation: $\mathbf{q} = \mathrm{DFT}[\mathbf{x}[\bar{k}]]$
11: AoA estimation: $\widehat{\varphi} = \arcsin(\frac{2}{N}\ \mathrm{argmax}_{i\in\{1,2,\ldots,N\}}\{|q_i|\})$

Start of ID detection

12: **for** $j = 1, 2, \ldots, K$ **do**
13: $k = k + 1$
14: Transmit: $\sqrt{P_\mathrm{T}}\,\mathbf{x}[\bar{k}]$
15: Receive: $\mathbf{y}[k] = e^{\jmath\phi[k]}\, \mathbf{A}^*(\varphi)\, \mathbf{x}^*[\bar{k}] + \mathbf{n}^*[k]$
16: Create the decision variable: $u[k] = \mathbf{x}^\dagger[\bar{k}]\,\mathbf{y}^*[k]$
17: Decode the symbol: $\widehat{\phi}[j] = \mathsf{demodulation}(-\arg\{u[k]\})$
18: **end for**
19: Extract the packet ID: $\{\widehat{\phi}[j]\}_{j=1,2,\ldots,K}$

End of ID detection

20: **end if**
21: **end for**

The decision variable $u[k] = \mathbf{x}^\dagger[k-1]\,\mathbf{y}^*[k]$, which depends on $e^{-\jmath\phi[k]}$, is then computed[5] (step 6) allowing also to estimate the signal-to-noise ratio (SNR) $\gamma[k] = |u[k]|^2/\sigma_w^2$ experienced in the current iteration by the MIMO TRX (step 7). If $\gamma[k]$ exceeds a specific detection threshold η_1, i.e., $\gamma[k] = |u[k]|^2/\sigma_w^2 > \eta_1$, and there is no significant increase in received power compared to the previous iteration, i.e., $\gamma[k]/\gamma[k-1] < \eta_2$, where η_1 and η_2 are empirically tuned thresholds, then the RAA is detected (step 8). In fact, the first inequality checks that a certain level of energy has been received compared to the noise level, whereas the second one guarantees that convergence is approximately reached.

If this is the case, the MIMO TRX assumes that the transient interval—during which the beamforming vector is iteratively

[5]In fact, in the absence of noise, it is easy to show from (12) that $u[k] = \mathbf{x}^\dagger[k-1]\,\mathbf{y}^*[k] \propto e^{-\jmath\phi[k]}$, being $\mathbf{x}^\dagger[k-1]\,\mathbf{x}[k-1] = 1$.

$$\mathbf{y}[k] = \underbrace{\sqrt{P_\mathrm{T}}\, g\, e^{\jmath\phi[k]} MNG_\mathrm{A}G_\mathrm{RAA}\left(\frac{\lambda}{4\pi d}\right)^2 \mathbf{v}^*(\varphi)\mathbf{v}^\top(\varphi)\mathbf{x}^*[k-1]}_{\tilde{\mathbf{y}}[k]\text{: useful term}} + \underbrace{g\,\sqrt{MNG_\mathrm{A}G_\mathrm{RAA}}\,\frac{\lambda}{4\pi d}\mathbf{v}^*(\varphi)\mathbf{u}^\dagger(\psi)\,\boldsymbol{\eta}^*[k] + \mathbf{w}[k]}_{\text{noise term}} \tag{13}$$

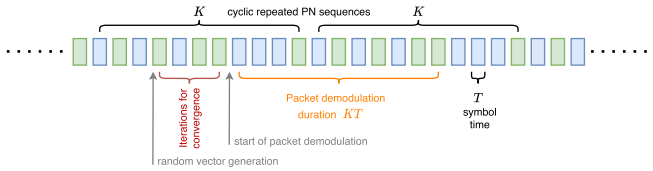

Fig. 5. Cyclic transmission of the RAA's ID. Time evolution.

adjusted to point toward the RAA—is over and that the vector is now accurately aligned with the RAA. Therefore, the current time index $\bar{k}$ is "frozen" (step 9) and the AoA estimation is carried out (steps 10 and 11). Specifically, the AoA estimate $\widehat{\varphi}$ of φ concerning the detected RAA is obtained as[6]

$$\widehat{\varphi} = \arcsin\left(\frac{2}{N}\ \mathrm{argmax}_{i\in\{1,2,\ldots,N\}}\left\{|q_i|\right\}\right) \tag{16}$$

where $\mathbf{q} = \{q_i\}$ is the Discrete Fourier Transform (DFT) of the beamforming vector corresponding to the detected RAA, that is

$$\mathbf{q} = \mathrm{DFT}\left[\mathbf{x}[\bar{k}]\right]\ . \tag{17}$$

To identify the detected RAA, the MIMO TRX must now extract its ID from the backscattered signal. To this end, we consider the RAA ID encoded in a unique pseudo noise (PN) sequence of length K symbols, which the RAA transmits cyclically by modulating the backscattered signal. Of course, only during the transmission of the interrogation signal from the MIMO TRX, such PN sequence corresponds to a physical modulated signal. In this regard, Fig. 5 shows the sequence of K symbols, out of a binary alphabet, that corresponds to the backscatter modulation cyclically realized at the RAA. The identification task is performed in steps 12 to 18, where the MIMO TRX:

- transmits always using the optimal beamforming vector $\mathbf{x}[i]$ (step 14);
- receives the backscattered signal carrying the ID information in $\phi[k]$ (step 15);
- creates the decision variable $u[k]$ (step 16);
- finally, determines the modulation symbol conveyed by $\phi[k]$ through a suitable demodulation scheme applied to $u[k]$, depending on the modulation alphabet (step 17).

Once all the K components of the ID have been collected (step 19), the MIMO TRX can finally assign an identity to the RAA transmitting from the direction given by the estimated AoA. According to this scheme and thanks to the correlation characteristic of the PN sequence, dedicated signaling for frame-level synchronization between the MIMO TRX and the RAA is not required.

Commentary: In the absence of noise and data, the processing presented corresponds to the *Power Method* which allows to estimate the strongest eigenvector of a square matrix $\mathbf{A}$, and it is described by the recursive relation [42]

$$\mathbf{x}[k] = \frac{\mathbf{A}\,\mathbf{x}[k-1]}{\|\mathbf{A}\,\mathbf{x}[k-1]\|} \tag{18}$$

where $\mathbf{x}[0]$ can be either an approximation of the top (dominant) eigenvector, if available, or a random unit norm vector. It results

[6]An array spacing $\Delta = \lambda/2$ is assumed.

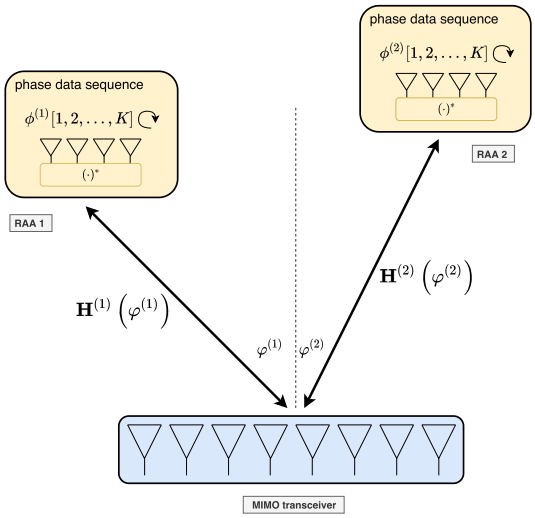

Fig. 6. Communication and AoA estimation with multiple RAAs sending packets of K bytes cyclically.

that, for $k \to \infty$, $\mathbf{x}[k]$ converges to the top eigenvector. Thus, $\mathbf{x}[k]$ tends to the direction φ of the top eigenvector of the *modified round-trip channel* $\mathbf{A}(\varphi)$ (i.e., $\mathbf{H}^{\dagger}\mathbf{H}$), i.e., the estimated angle converges to the AoA of the signal from the RAA.

In summary, the iterative process proposed here enables the MIMO TRX to transmit according to the optimal beamforming vector pointing toward the RAA. As a result, the AoD of the signal from the MIMO TRX coincides with the AoA of the signal received from the RAA, thus enabling angle-based localization. This is achieved by exploiting the processing gain offered by the N antennas at the MIMO TRX and the M antennas at the RAA, but without explicit channel estimation, and utilizing backscattering.

C. Extension to Multiple RAA-Based Devices

Let us now assume that there are P RAA-based devices in the environment. These devices can either be mobile UEs in Architecture 1 or fixed anchors in Architecture 2. In the same environment, there are also devices equipped with a standard antenna array (MIMO TRX), which emit interrogation signals to detect the presence of the P RAA-based devices and estimate their corresponding AoAs (see Fig. 6).

In LOS channel conditions, the process of detecting the presence of the P RAAs by a MIMO TRX is equivalent to determining the top eigenvectors of the P channels $\mathbf{A}^{(p)}, p = 1, 2, \ldots, P$, between the MIMO TRX and the P RAAs. In particular, (12) becomes

$$\mathbf{y}[k] = \sum_{p=1}^{P}\left(e^{-\jmath\phi^{(p)}[k]}\,\mathbf{A}^{(p)}\left(\varphi^{(p)}\right)\right)^{*}\mathbf{x}^{*}[k-1] + \mathbf{n}^{*}[k] \tag{19}$$

where $\{\phi^{(p)}[k]\}$ and $\varphi^{(p)}$ are, respectively, the information data and the AoA associated with the p-th RAA.

In this regard, the iterative scheme proposed in Section III-B, which is limited to the estimation of only the top eigenvector, can be extended to estimate the P top eigenvectors of $\mathbf{A} = \sum_{p=1}^{P} \mathbf{A}^{(p)}(\varphi^{(p)})$, as described in the following. Unfortunately, the top eigenvectors of $\mathbf{A}$, in general, do not correspond exactly to the top eigenvectors of the single matrices $\mathbf{A}^{(p)}$ composing it unless the channels are orthogonal. Nevertheless, if the RAAs are positioned at distinct angles and the number of antennas is increased by employing massive arrays (massive MIMO), the channels $\mathbf{A}^{(p)}$ tend to become orthogonal. This situation approaches the so-called *favorable propagation* [43], which, strictly speaking, occurs when the channels $\mathbf{A}^{(p)}$ are orthogonal [44]. Under this condition, once the top eigenvector of $\mathbf{A}$ has been estimated, the detection of the second top eigenvector can be achieved using the same scheme described in Section III-B, provided that the iterative search is conducted in a space orthogonal to that spanned by the top eigenvector. To elaborate further, let's consider a matrix $\mathbf{B}$ that collects all the previously discovered top eigenvectors. At Step 5 of the algorithm described in Section III-B, the following operation is performed:

$$\mathbf{x}[k] = \frac{\left(\mathbf{I} - \mathbf{B}\,\mathbf{B}^{\dagger}\right)\mathbf{y}^{*}[k]}{\left\|\left(\mathbf{I} - \mathbf{B}\,\mathbf{B}^{\dagger}\right)\mathbf{y}^{*}[k]\right\|} \tag{20}$$

so that, before further processing, the updated beamforming vector $\mathbf{x}[k]$ is adjusted to be orthogonal to $\mathbf{B}$. This ensures that the subsequent search is conducted within the null space of $\mathbf{B}$, preventing the detection of previously identified eigenvectors (i.e., already detected RAA-based devices).

In a more general scenario where the favorable propagation condition is not perfectly achieved, the top eigenvectors of $\mathbf{A}$ may not precisely align with the top eigenvectors of $\mathbf{A}^{(p)}$ [34], [45]. This can result in interference among RAA-based devices and subsequent performance degradation for demodulation and AoA estimation. We underline, however, that this effect is considered in our numerical results. Finally, we note that this issue is not unique to our solution. Rather, it affects conventional multi-user MIMO systems in general.

IV. Convergence Analysis

In the following, we analyze the convergence of the proposed iterative scheme to the optimal beamforming vector in the presence of data modulation and noise, by showing the time evolution of the SNR at the MIMO TRX. Then, we consider a dynamic scenario with the RAA moving along a certain trajectory, and we discuss a channel tracking strategy to speed up the convergence and the performance. For the sake of simplicity in notation, we consider only one RAA-based node, although the same results apply in scenarios with multiple RAAs, provided that the channels are orthogonal due to favorable propagation conditions.

For convenience, let us introduce the eigenvalue decomposition of matrix $\mathbf{A}$, which we consider now a generic modified round-trip channel matrix, as

$$\mathbf{A} = \mathbf{V}\mathbf{\Lambda}\mathbf{V}^{\dagger} = \sum_{j=1}^{N} \lambda_j\, \mathbf{v}_j\, \mathbf{v}_j^{\dagger} \tag{21}$$

where $\mathbf{\Lambda} = \mathrm{diag}(\lambda_1, \lambda_2, \ldots, \lambda_N)$, being λ_j the j-th eigenvalue with $\lambda_1 \geq \lambda_2 \geq \ldots, \geq \lambda_N$, and $\mathbf{v}_j$ is the j-th eigenvector (direction) forming the j-th column of matrix $\mathbf{V} \in \mathbb{C}^{N\times N}$. As a consequence, the generic vector $\mathbf{x}[k]$ at the k-th iteration can be decomposed as

$$\mathbf{x}[k] = \sum_{j=1}^{N} x_j[k]\, \mathbf{v}_j \tag{22}$$

being $x_j[k] = \mathbf{v}_j^{\dagger}\,\mathbf{x}[k]$ the projection of $\mathbf{x}[k]$ onto the j-th direction $\mathbf{v}_j$. Similarly, the noise term can be expressed as

$$\mathbf{n}[k] = \sum_{j=1}^{N} n_j[k]\, \mathbf{v}_j \tag{23}$$

where $n_j \sim \mathcal{CN}(0, \sigma_j^2)$, with

$$\sigma_j^2 = \sigma_w^2 + \frac{\lambda_j\, g\, \sigma_\eta^2}{\sqrt{P_{\mathrm{T}}}}\,. \tag{24}$$

In the following analysis, we assume that the noise generated by the RAA, which is transmitted back toward the MIMO TRX, is negligible at the receivers' side compared to its own noise, i.e., $\sigma_j^2 \simeq \sigma_w^2$, $\forall j$. This is reasonable considering it is attenuated by the MIMO TRX-RAA channel.

A. Convergence and SNR Evolution

We now assess the SNR in the k-th iteration of the scheme aimed at estimating the top eigenvector of the channel. This SNR affects both the demodulation of the data symbol conveyed by $\phi[k]$ and the estimation of the angle $\varphi[k]$.

As per Step 5 of the scheme described in Section III-B, the beamforming vector $\mathbf{x}[k]$ at the k-th iteration is given by:

$$\mathbf{x}[k] = \frac{\mathbf{y}^{*}[k]}{\|\mathbf{y}[k]\|} = \frac{\mathbf{A}\, e^{-\jmath\phi[k]}\mathbf{x}[k-1] + \mathbf{n}[k]}{\left\|\mathbf{A}\, e^{-\jmath\phi[k]}\mathbf{x}[k-1] + \mathbf{n}[k]\right\|} \tag{25}$$

where

$$\mathbf{y}^{*}[k] = \sum_{j=1}^{N} \mathbf{v}_j \left(\lambda_j x_j[k-1] e^{-\jmath\phi[k]} + n_j[k]\right)\,. \tag{26}$$

According to step 6 in Section III-B, the decision variable $u[k]$ at the k-th symbol is

$$\begin{aligned} u[k] &= \mathbf{x}^{\dagger}[k-1]\,\mathbf{y}^{*}[k] \\ &= \mathbf{x}^{\dagger}[k-1]\,\mathbf{A}\, e^{-\jmath\phi[k]}\mathbf{x}[k-1] + \mathbf{x}^{\dagger}[k-1]\,\mathbf{n}[k] \\ &= e^{-\jmath\phi[k]} \sum_{j=1}^{N} \lambda_j \left|x_j[k-1]\right|^2 + \mathbf{x}^{\dagger}[k-1]\,\mathbf{n}[k] \end{aligned} \tag{27}$$

in which the first term is the useful one, as it contains the phase $\phi[k]$, and the second term represents the noise.

Considering that by construction $\|\mathbf{x}[k]\|^2 = 1$, the SNR in (27) at the k-th time interval is

$$\mathsf{SNR}_{\mathrm{dec}}[k] = \frac{\left(\sum_{j=1}^{N} \lambda_j \left|x_j[k-1]\right|^2\right)^2}{\sigma_w^2}\,. \tag{28}$$

Note that $|x_j[k-1]|^2/\|\mathbf{x}[k-1]\|^2 = |x_j[k-1]|^2$ represents the fraction of the total power transmitted by the MIMO TRX associated with direction $\mathbf{v}_j$ at the discrete time $k-1$. Then, at the end of the k-th time interval, the SNR at the MIMO TRX along the direction $\mathbf{v}_j$ is given by

$$\mathsf{SNR}_j[k] = \frac{\lambda_j^2\,|x_j[k-1]|^2}{\sigma_w^2}\,. \tag{29}$$

Therefore, we can rewrite (28) as a function of $\mathsf{SNR}_j[k]$ as

$$\mathsf{SNR}_{\text{dec}}[k] = \left(\sum_{j=1}^{N}\frac{\mathsf{SNR}_j[k]}{\sqrt{\mathsf{SNR}_{j,\max}}}\right)^2 \tag{30}$$

where $\mathsf{SNR}_{j,\max} = \frac{\lambda_j^2}{\sigma_w^2}$ represents the maximum possible SNR along the direction $\mathbf{v}_j$, i.e., the SNR the receiver would experience if all the power were concentrated in the direction $\mathbf{v}_j$. The goal is to determine an iterative expression for $\mathsf{SNR}_{\text{dec}}[k]$ and evaluate the convergence condition of the iterative scheme proposed. Considering (26), the fraction of the total power that is associated with direction $\mathbf{v}_j$ at the beginning of time interval k can be written as

$$|x_j[k]|^2 = \frac{\lambda_j^2\,|x_j[k-1]|^2 + \sigma_w^2}{\sum_{i=1}^{N}\left(\lambda_i^2\,|x_i[k-1]|^2 + \sigma_w^2\right)}\,. \tag{31}$$

Then, by inverting (29) and plugging $|x_j[k]|^2$ at both the left-hand and right-hand sides of (31), we obtain the following iterative formula for $\mathsf{SNR}_j[k]$

$$\begin{aligned}\mathsf{SNR}_j[k] &= \frac{\lambda_j^2\,(\mathsf{SNR}_j[k-1]+1)}{\sigma_w^2\left[\sum_{i=1}^{N}(\mathsf{SNR}_i[k-1]+1)\right]}\\ &= \mathsf{SNR}_{j,\max}\frac{\mathsf{SNR}_j[k-1]+1}{N+\sum_{i=1}^{N}\mathsf{SNR}_i[k-1]}\end{aligned} \tag{32}$$

for $k \geq 2$, where

$$\mathsf{SNR}_j[1] = \mathsf{SNR}_{j,\max}\,|x_j[0]|^2\,. \tag{33}$$

The recursive expression (32) can be numerically evaluated to obtain the SNR evolution for each direction. Therefore, it is of interest to investigate whether convergence toward the top eigenvector is guaranteed, and under what conditions. Denote by $r = \text{rank}(\mathbf{A})$ the rank of matrix $\mathbf{A}$, i.e., the rank of the channel. Unfortunately, a general convergence analysis appears prohibitive for a channel with a generic rank. As a consequence, we derive in the following a convergence condition valid for a rank-1 channel and show numerically that the same result holds also for higher-rank channels. Then, assuming an ideal free-space LOS channel for AoA estimation as in (8), we have only $\lambda_1 \neq 0$, thus (30) is given by

$$\mathsf{SNR}_{\text{dec}}[k] = \frac{(\mathsf{SNR}_1[k])^2}{\mathsf{SNR}_{1,\max}} \tag{34}$$

with the SNR at the k-th time interval along direction $\mathbf{v}_1$ in (32) expressed as

$$\mathsf{SNR}_1[k] = \mathsf{SNR}_{1,\max}\frac{\mathsf{SNR}_1[k-1]+1}{N+\mathsf{SNR}_1[k-1]}\,. \tag{35}$$

This case allows an easy evaluation of the convergence value. In fact, the solution at the equilibrium of the recursive expression in (35) can be found by imposing that $\mathsf{SNR}_1[k] = \mathsf{SNR}_1[k-1] = x$ and solving the following second-order equation

$$x = \mathsf{SNR}_{1,\max}\frac{x+1}{x+N}\,. \tag{36}$$

By considering only the positive solution, the condition on the final convergence value is:

- If $\mathsf{SNR}_{1,\max}/N \gg 1$, at the convergence it is $\mathsf{SNR}_1[k] \simeq \mathsf{SNR}_{1,\max}$ and hence, from (34), $\mathsf{SNR}_{\text{dec}}[k] \simeq \mathsf{SNR}_{1,\max}$, which takes the role of asymptotic SNR corresponding to the optimal beamforming vector for a channel with $r = 1$.
- If $\mathsf{SNR}_{1,\max}/N \ll 1$, we still have convergence but with $\mathsf{SNR}_{\text{dec}}[k] \ll 1$ thus unable of guaranteeing a suitable data demodulation and AoA estimation performance.

Due to the previous result, we define the value $\mathsf{SNR}_{1,\text{boot}} = \mathsf{SNR}_{1,\max}/N$ as *bootstrap SNR*. It is worth noticing that the convergence is always achieved to a convergence value which depends on the condition on the bootstrap SNR above, but it does not depend on the initial value $\mathbf{x}[0]$.

Assuming the MIMO transmitter and the RAA are in paraxial LOS configuration (i.e., parallel arrays with $\varphi = \psi = 0$), the first eigenvalue of $\mathbf{A}$ is, according to (9), $\lambda_1 = \sqrt{P_{\text{T}}}g\sigma_1^2$ and the maximum and bootstrap SNRs become, respectively,

$$\mathsf{SNR}_{1,\max} = \frac{P_{\text{T}}\,g^2\,N^2\,M^2\,G_{\text{A}}^2\,G_{\text{RAA}}^2\,\lambda^4}{\sigma_w^2\,(4\pi\,d)^4} \tag{37}$$

$$\mathsf{SNR}_{1,\text{boot}} = \frac{P_{\text{T}}\,g^2\,N\,M^2\,G_{\text{A}}^2\,G_{\text{RAA}}^2\,\lambda^4}{\sigma_w^2\,(4\pi\,d)^4}\,. \tag{38}$$

According to the last equations, increasing N and M is beneficial for improving the link budget but also for the bootstrap SNR; however, M has a higher impact than N thus, in general, it is more convenient to increase the RAA size to improve the performance.

1) Numerical Example: To show the convergence behavior analyzed above, we provide a numerical example for an array at the MIMO TRX with $N = 100$ elements and a rank-3 channel with two different configurations:

- *Configuration a)* $\mathsf{SNR}_{1,\max} = 25$ dB, $\mathsf{SNR}_{2,\max} = 17\,dB$, $\mathsf{SNR}_{3,\max} = 13\,dB$, corresponding to $\mathsf{SNR}_{1,\text{boot}} = 5\,dB$;
- *Configuration b)* $\mathsf{SNR}_{1,\max} = 15\,dB$, $\mathsf{SNR}_{2,\max} = 10\,dB$, $\mathsf{SNR}_{3,\max} = 5\,dB$, corresponding to $\mathsf{SNR}_{1,\text{boot}} = -5\,dB$.

The initial precoding vector $\mathbf{x}[0]$ is randomly chosen at the startup, therefore it is $|x_j[0]|^2 \simeq 1/N$ and $\mathsf{SNR}_1[1] \simeq \mathsf{SNR}_{1,\max}/N$. Other initial strategies will be discussed in the next section.

In Fig. 7, the evolution of $\mathsf{SNR}_j[k]$, $j = 1, 2, 3$, using (32) is shown for the 2 configurations. From the plots, it can be noticed that when $\mathsf{SNR}_{1,\text{boot}} > 0\,dB$ the SNR associated with the top eigenvector ($j = 1$) converges to $\mathsf{SNR}_{1,\max}$, given by (37), within 5-6 time intervals, whereas it converges to very low values when $\mathsf{SNR}_{1,\text{boot}} < 0\,dB$, as well predicted by the convergence condition even though it has been derived assuming a rank-1

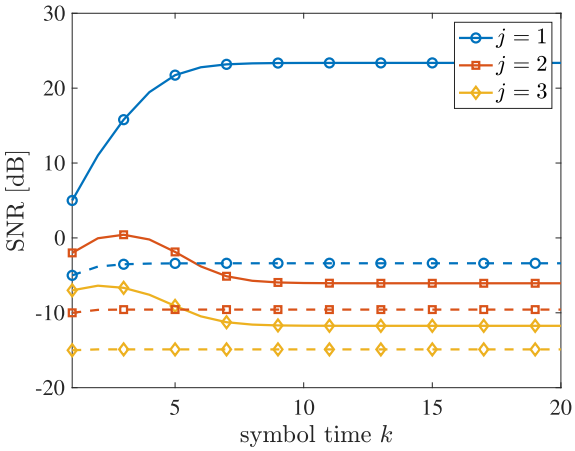

Fig. 7. Evolution of $\mathsf{SNR}_j[k]$, $j=1,2,3$ as a function of the time interval k for a rank-3 channel with two different configurations. Continuous lines (–) are for *configuration a)* ($\mathsf{SNR}_{1,\text{boot}} > 0\,dB$); Dashed lines (- -) are for *configuration b)* ($\mathsf{SNR}_{1,\text{boot}} < 0\,dB$).

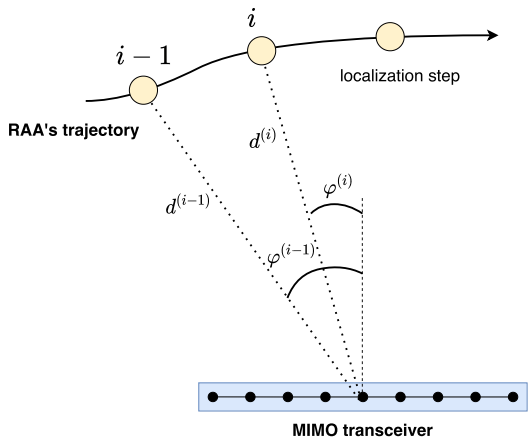

Fig. 8. Localization of the RAA in a dynamic scenario.

channel. In fact, in any case the SNR of the components of $\mathbf{x}[k]$ associated with the second and third eigenvectors, $\mathsf{SNR}_2[k]$ and $\mathsf{SNR}_3[k]$, tend to negligible values, i.e., the proposed scheme always converges to the top eigenvector but with a final SNR depending on $\mathsf{SNR}_{1,\text{boot}}$.

According to the analysis outlined above, the convergence of the proposed scheme to $\mathsf{SNR}_{1,\max}$ (i.e., to the largest SNR) is ensured only if the bootstrap SNR significantly exceeds one. Therefore, the system must be properly designed, paying particular attention to factors such as the number of antennas, transmitted power, and RAA gain relative to the operating distance, to ensure that this condition is likely satisfied.

B. Channel Tracking

Consider now the localization task in a dynamic scenario, where one of the two nodes (e.g., the RAA) moves along a certain trajectory (see Fig. 8). The iterative scheme described in Section III is executed at specific points of the trajectory, namely, the localization steps. Specifically, at the i-th localization step an AoA estimate (after RAA detection) and a data packet consisting of K symbols (e.g., the node's ID) are obtained. Referring to Fig. 8, the RAA is observed at an angle $\varphi^{(i)}$ with respect to the MIMO TRX and located at a distance $d^{(i)}$ during the i-th localization step. Notice that, in this section, we use here the notation $(\cdot)^{(i)}$ to indicate the quantities at the i-th localization step, thus without accounting for multiple RAAs as in Section III-C for the sake of simplicity. Specifically, τ denotes the time interval between two consecutive localization steps. Thus, we can define the maximum localization update rate as $\mathcal{R}=1/\tau$, assuming that a sufficient number of angular measurements is collected at the i-th localization step to obtain an unambiguous location estimate.

To speed up the convergence of the proposed iterative scheme, rather than randomly choosing an initial beamforming vector $\mathbf{x}^{(i)}[0]$ at the i-th localization step, it may be more convenient to use the last available estimated beamforming vector $\mathbf{x}^{(i-1)}[\bar{k}]$ at the previous localization step (i.e., $i-1$), thus assuming $\mathbf{x}^{(i)}[0]=\mathbf{x}^{(i-1)}[\bar{k}]$. Since, according to this choice, the estimated beamforming vectors are re-used and updated iteratively during the movement of the node, we define such a strategy as *channel tracking*. In the following, we will evaluate the conditions under which performing channel tracking is advantageous.

Let us now define, for further convenience, the SNR along the first direction at the startup for the i-th localization step; this is the key parameter determining the convergence speed of the scheme. Specifically, we define it as *startup SNR* so that $\mathsf{SNR}^{(i)}_{\text{start}}=\mathsf{SNR}^{(i)}_{1}[0]$ for the localization step i. We assume that at the localization step $i-1$ the convergence to $\mathsf{SNR}_{1,\max}$ was achieved. Let us also now consider that the last beamforming vector $\mathbf{x}^{(i-1)}[K]$ of localization step $i-1$ is used as first beamforming vector $\mathbf{x}^{(i)}[0]$ of localization step i. In such a case, the SNR along the first direction at the startup for the localization step i, which determines the convergence speed, can be written as

$$\mathsf{SNR}^{(i)}_{\text{start}}=\gamma\,\mathsf{SNR}^{(i-1)}_{1,\max} \tag{39}$$

where γ reflects the change in the SNR between the two positions when adopting the previous beamforming vector. In particular, we can decompose γ as the product of two factors, i.e., $\gamma=\xi\rho$; the coefficient $\rho\leq 1$ indicates the correlation between the channels related to the localization steps $i-1$ and i, while $\xi \lesseqgtr 1$ indicates the difference in terms of path loss. The term ρ can be obtained as the cross-correlation coefficient between the beamforming vectors corresponding to angles $\varphi^{(i-1)}$ and $\varphi^{(i)}$, that are, $\mathbf{v}(\varphi^{(i-1)})$ and $\mathbf{v}(\varphi^{(i)})$ as

$$\rho=\left|<\mathbf{v}(\varphi^{(i)}),\mathbf{v}(\varphi^{(i-1)})>\right|. \tag{40}$$

The term ξ can be written as the ratio between the path loss at positions $i-1$ and i, thus we have $\xi=\mathcal{L}(d^{(i-1)})/\mathcal{L}(d^{(i)})$ according to (15) when considering a free space scenario. If $\mathsf{SNR}^{(i)}_{1,\max}/N\gg 1$ we have convergence at the maximum SNR for the localization step i, which is $\mathsf{SNR}^{(i)}_{1,\max}=\xi\,\mathsf{SNR}^{(i-1)}_{1,\max}$.

The choice of using the previous convergence beamforming vector is beneficial only if the corresponding startup SNR is larger than that obtained with the random guess $\mathbf{x}^{(i)}[0]$ at the i-th localization step. In fact, when selecting randomly

the first beamforming vector $\mathbf{x}^{(i)}[0]$, we obtain the value $\mathsf{SNR}^{(i)}_{1,\text{boot}} = \mathsf{SNR}^{(i)}_{1,\text{max}}/N$ as the starting point of the iterative procedure. Formalizing, the choice is beneficial if

$$\mathsf{SNR}^{(i)}_{\text{start}} = \xi\rho\,\mathsf{SNR}^{(i-1)}_{1,\text{max}} > \mathsf{SNR}^{(i)}_{1,\text{boot}} = \frac{\mathsf{SNR}^{(i)}_{1,\text{max}}}{N}\,. \tag{41}$$

However, since it holds that $\mathsf{SNR}^{(i)}_{1,\text{max}} = \xi\,\mathsf{SNR}^{(i-1)}_{1,\text{max}}$ (i.e., the SNR obtained when considering the optimal beamforming vector at each location) the criterion (41) becomes

$$\rho > \frac{1}{N}\,. \tag{42}$$

It is very important to underline that the convenience is experienced in the number of iterations needed to reach convergence (i.e., convergence speed); no differences are obtained in terms of probability of convergence to the maximum SNR, since this is determined only by the bootstrap SNR value.

From (42), it could be inferred that a large number of antennas N at the MIMO TRX is beneficial for ensuring faster convergence (i.e., that a larger number of antennas can allow to tolerate highly decorrelated channels between localization steps $i-1$ and i). However, it is important to note that the correlation coefficient ρ itself strongly depends on the number of antennas N. For instance, consider a scenario where there is a small movement of the RAA orthogonal to the MIMO TRX's array normal direction. In such a case, the primary source of change in the SNR arises from the differing optimal combinations of phase values at the two positions, leading to $\gamma \approx \rho$. Consider for simplicity $\varphi(i-1) = 0$ (i.e., RAA on the MIMO TRX's normal direction at localization step $i-1$), and the RAA moving with constant speed v transversal to the MIMO TRX's normal direction. When operating with half-wavelength spaced ULAs, we have

$$\begin{aligned}\mathbf{v}_1^{(i-1)} &= \frac{1}{\sqrt{N}}\,[1,1,\dots 1] \;\in \mathbb{C}^{N\times 1}\\ \mathbf{v}_1^{(i)} &= \frac{1}{\sqrt{N}}\left[1, e^{\jmath\pi\sin\varphi^{(i)}},\dots,e^{\jmath\pi(N-1)\sin\varphi^{(i)}}\right] \;\in \mathbb{C}^{N\times 1}\end{aligned} \tag{43}$$

thus we can write

$$\rho = \frac{1}{N}\left|\sum_{n=0}^{N-1} e^{-\jmath\pi n\sin\varphi^{(i)}}\right| \approx \operatorname{sinc}\left(\frac{N\sin\varphi^{(i)}}{2}\right). \tag{44}$$

In order to obtain a simple condition for determining the advantage of using the previous beamforming vector in the dynamic scenario, we can approximate the sinc function using its Taylor expansion around the origin, i.e., $\operatorname{sinc}(x) \approx 1 - \frac{\pi^2 x^2}{3!}$ and consider $\sin\varphi^{(i)} \approx \tan\varphi^{(i)} = v\tau/d^{(i)}$ obtaining for (42)

$$1 - \frac{\pi^2 N^2 v^2 \tau^2}{24\left(d^{(i)}\right)^2} > \frac{1}{N}\,. \tag{45}$$

Then, by inverting (45), we get that the choice of using the previous beamforming vector is beneficial with respect to a random guess to ensure faster convergence only if

$$v < \frac{2d^{(i)}\sqrt{6(N-1)}}{\pi\tau N\sqrt{N}}\,. \tag{46}$$

When such a condition is not met, the channel variations between localization steps $i-1$ and i are too significant, and relying on the previous beamforming vector proves ineffective. In such cases, a random guess can ensure faster convergence.

According to (46), the larger the number of antennas N, the lower the maximum tolerated speed. In fact, a large number of antennas causes the channel to quickly decorrelate when moving from one position to another. Interestingly, it is worth noting that the convergence speed is not affected by M, i.e., the number of antennas at the RAA. Thus, this parameter can be increased to improve the link budget without encountering convergence constraints in dynamic scenarios.

1) Numerical Example: In order to characterize the potential of tracking the channel by exploiting the last available beamforming vector, we consider a numerical example considering a variable number N of antennas and $\tau = 100$ ms. Fig. 9 shows the maximum speed for the RAA in order to benefit from using the previous beamforming vector according to (46). It is possible to notice that, as the number of antennas increases, the maximum speed decreases. Moreover, if the RAA is close to the MIMO TRX the speed limit is lower since the channel changes faster its angular correlation (larger variation in angle φ for a given transversal movement). It is worth noticing that if the speed is larger than that reported in Fig. 9, convergence is still guaranteed if the bootstrap SNR satisfies $\mathsf{SNR}^{(i)}_{\text{start}}/N \gg 1$; however, using a random guess would be more effective (higher startup SNR thus faster convergence).

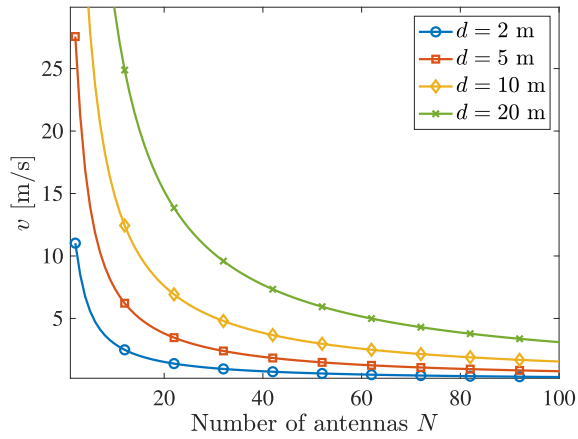

Fig. 9. Maximum speed to make the channel tracking effective for improving the convergence speed of the proposed scheme.

V. Numerical Results

In this section, we investigate the performance of the proposed localization strategies for both Architecture 1 and Architecture 2. The simulation parameters, detailed below, are identical in both cases.

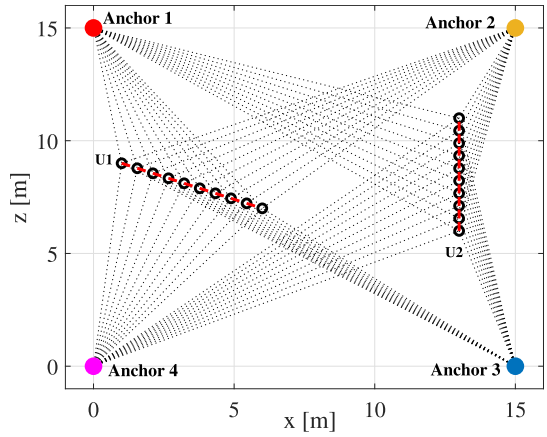

Fig. 10. Simulated scenario: Two users (U1 and U2) moving along the red trajectories, and four anchors. Black circles indicate the locations corresponding to the localization steps given a certain localization update rate $\mathcal{R}$.

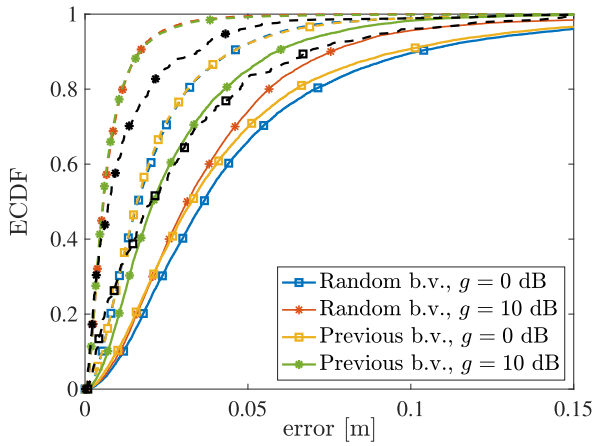

Fig. 11. ECDF of the absolute localization error for Architecture 1. Dashed lines (- -) are for the free-space LOS channel; Continuous lines (–) are for the 3GPP CDL-E channel. Black lines represent the simulated effect of clutter by applying a random beamforming vector.

TABLE I
PARAMETERS USED IN THE SIMULATIONS

Parameter	Symbol	Value
Carrier frequency	f_c	28 GHz
Bandwidth	W	10 MHz
Symbol time	T	190 ns
TX power	P_T	0 dBm
Path loss exponent	β	2
MIMO TRX antenna gain	G_A	0 dBi (isotropic)
RAA antenna gain	G_{RAA}	0 dBi (isotropic)
RAA backscatter gain	g	0 dB or 10 dB
RAA/MIMO TRX noise figure	F	3 dB
RAA antenna elements	M	20×20 (10.7×10.7 cm^2)
MIMO TRX antenna elements	N	10×10 (5.36×5.36 cm^2)
SNR detection threshold	η_1	30 dB
SNR convergence threshold	η_2	3 dB
ID length	K	40 symbols
Localization update time-step	τ	100 ms
Speed of UEs	v	0.54 m/s
UE's trajectory length	L	5.39 m

A. Simulated Scenario

Simulations are performed in the 2D scenario depicted in Fig. 10, where two UEs (U1 and U2) move along the red trajectories in the $x-z$ plane. Four anchors are also positioned in this scenario. The RAAs, whether at the UE side or the anchor side depending on the architecture being investigated, consist of square uniform planar arrays with 20×20 antenna elements arranged in the $x-y$ plane. MIMO TRXs consist also of uniform planar arrays featuring 10×10 antenna elements, deployed in the $x-y$ plane.

According to the scheme outlined in Section III-B, MIMO TRXs employ the signals backscattered by the RAAs to estimate their AoAs. Notice that, despite localization is realized on a plane, both fixed and mobile antennas (including RAAs) are assumed as 2D panels; this choice does not affect the angular resolution but improves the link budget thanks to additional SNR gain. The parameters used in the simulations, unless otherwise specified, are reported in Table I.

B. Localization Error Analysis - Architecture 1

Depending on the channel condition and SNR, one or more anchors (i.e., MIMO TRXs) in the scenario can detect the presence of the RAAs (i.e., UEs) at each localization step and obtain the associated AoA estimates. Then, the AoA estimates are fused using a least-square approach as described in [46], yielding an estimate $\widehat{\mathbf{p}}=[\widehat{x},\widehat{z}]$ of the position $\mathbf{p}=[x,z]$, in accordance with the geometry depicted in Fig. 10.

As a preliminary assessment of the proposed system performance, we conducted Monte Carlo simulations with a single UE (U1 in Fig. 10). The results are reported in Fig. 11, which shows the empirical cumulative distribution function (ECDF) of the absolute localization error $\epsilon=|\widehat{\mathbf{p}}-\mathbf{p}|$ under different conditions, obtained over 100 Monte Carlo iterations. Specifically, we considered a user moving with a speed of $v=0.54\,m/s$ along a straight trajectory of length $L=5.39\,m$, and a localization update rate $\mathcal{R}=10\,Hz$ (i.e., $\tau=100\,ms$), thus corresponding to 100 discrete localization steps along the trajectory. The results refer to various operating conditions, including:

- An ideal LOS channel (free-space) and a realistic 3GPP CDL-E channel [47];
- The exploitation of passive ($g=0\,dB$) and active ($g=10\,dB$) RAAs;
- The adoption of a random beamforming vector (b.v. in the plot legends) as initialization of the proposed scheme, or the last available beamforming vector, according to the channel tracking strategy presented in Section IV-B.

When focusing on the impact of the channel, it is evident from Fig. 11 that the best performance is achieved with free-space LOS conditions (dashed lines), owing to the absence of multipath propagation. In this case, deviations in the AoA estimate from the true angle primarily result from measurement noise. Performance deteriorates slightly when considering the 3GPP CDL-E channel (continuous lines), due to multipath effects. Generally, the localization error remains below 5 cm and 10 cm in 90% of cases for the free-space channel (dashed lines) and CDL-E channel (continuous line), respectively. The same figure also illustrates the impact of path loss on performance. It is evident that leveraging active RAAs (red/green lines) reduces the localization error, primarily due to increased received power and consequently more robust AoA estimation.

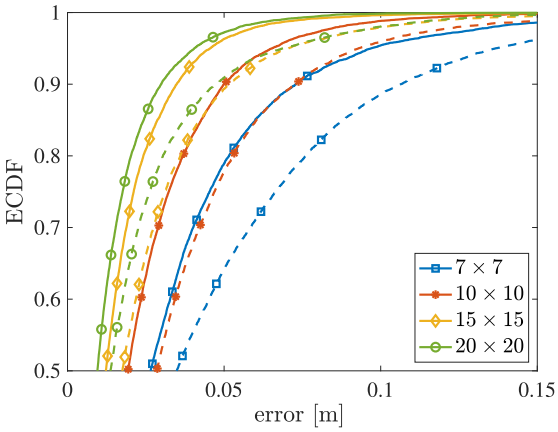

Fig. 12. ECDF of the absolute localization error for U1 (continuous lines) and U2 (dashed lines) in Architecture 1, varying the size $M \times M$ of the RAA.

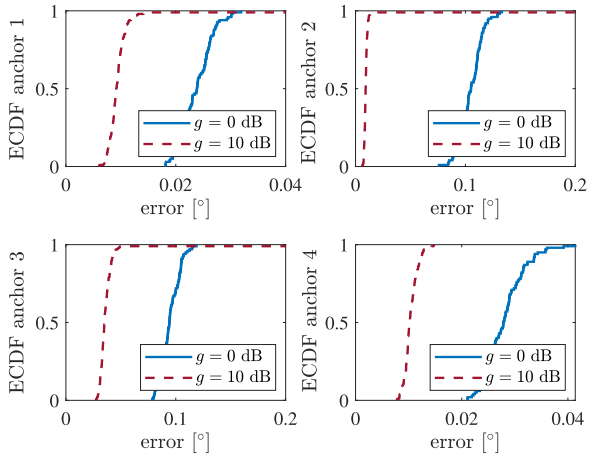

Fig. 13. ECDF of the angle estimation error in Architecture 2 for U1.

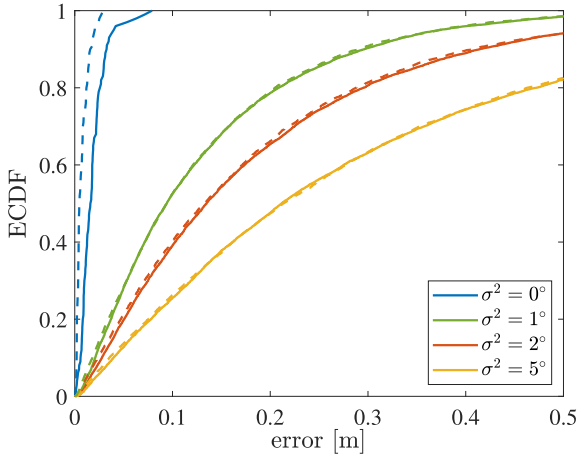

Fig. 14. ECDF of the absolute localization in Architecture 2, considering a residual random error with variance σ^2 on the UE orientation. Continuous lines (–) are for $g = 0\,dB$; Dashed lines (- -) are for $g = 10\,dB$.

When considering the channel tracking mechanism proposed in Section IV-B, no differences in performance are observed for the free-space LOS channel. This is expected, as channel tracking primarily facilitates faster convergence compared to randomly generating the initial beamforming vector. However, this aspect is not captured by the results shown in Fig. 11, which concern positioning errors. Contrarily, when a realistic multipath channel is considered, leveraging the previous beamforming vector (i.e., utilizing the channel tracking mechanism) results in a reduction in localization error. In fact, when the beamforming vector is randomly generated at each localization step, there is a chance that the AoA estimator locks onto a multipath component, potentially leading to more significant errors compared to starting the iterative algorithm from the previous, possibly correct, AoA estimate. According to [34], the effect of clutter on the algorithm is binary: below a certain threshold, it has no impact, but above the threshold the algorithm fails, making the user unobservable. Clutter intensity depends on factors like antenna number, transmitted power, and the specific scenario, making accurate modeling challenging. Instead of simulating clutter directly, we characterize its effect through the introduction of a link blockage probability p_c. Fig. 11 illustrates this effect, showing a 70% clutter probability simulated for $g = 0$ dB and $g = 10$ dB in a free-space LOS channel. As it can be observed, even in the presence of a high probability of blockage the localization performance degradation is limited mainly because of the diversity offered by the 4 anchor nodes. The impact of the array size on the AoA estimation and, consequently, on localization accuracy is shown in Fig. 12, which depicts the ECDF of the absolute localization error as the number of RAA elements varies. The simulations are carried out for both users moving along the trajectories shown in Fig. 10. Performance improves with an increasing number of antenna elements, due to the dual benefits of higher SNR (larger number of observations with additional antenna elements) and a larger aperture, which results in enhanced angular resolution.

C. Localization Error Analysis - Architecture 2

When considering Architecture 2, it is the UE that transmits the interrogation signal, which is then backscattered by RAA-equipped anchors. Therefore, it is the UE that estimates the AoA of the received signals relative to its own reference system. In this section, we focus on Architecture 2 and we investigate the performance of our localization strategy in the scenario depicted in Fig. 10, concentrating on U1. In Fig. 13, the ECDF of the absolute angle estimation error relative to each of the 4 anchors is shown. This figure was obtained with 100 Monte Carlo cycles along the trajectory, varying the gain of the backscattered signal g, with a LOS channel, and without utilizing the beamforming vector from the previous step. Fig. 13 shows that the accuracy of angular estimation is generally below one degree with the proposed setup. The highest accuracy is achieved by anchors 1 and 4, which are closest to U1. As for Architecture 1, increasing the gain g of the RAAs significantly reduces the error.

Regarding the estimation of the UE's position in Architecture 2 according to a global reference system, we have already pointed out that this is possible only if the UE knows the coordinates of the anchors and its own orientation. Fig. 14 shows the ECDF of the absolute localization error when assuming that the UE experiences a residual random error on its own orientation, obtained from external sensors. Specifically, this error is modeled as Gaussian with zero mean and variance σ^2. As it can be noticed, increasing the UE orientation error

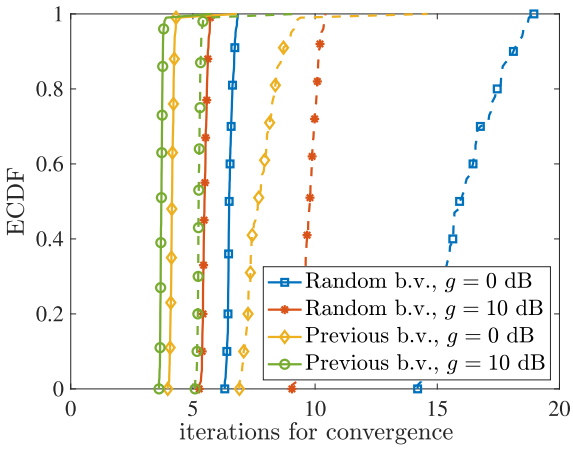

Fig. 15. Number of iterations required for detection relative to anchor 4, by varying the RAA gain and the use of the previous/random beamforming vector. Dashed lines (- -) are for U2; Continuous lines (–) are U1.

deteriorates the performance due to the mismatch between the local and global reference systems. While higher RAA gain g can be adopted in general to ameliorate the performance in the absence of residual orientation error ($\sigma^2 = 0°$), the presence of an orientation error outweighs the benefits of the RAA gain (the corresponding curves are overlapped for $\sigma^2 > 0°$ in Fig. 14). The blue curves also demonstrate that the two architectures exhibit a comparable performance.

D. Convergence Analysis

The impact of the channel tracking mechanism, introduced in Section IV-B, is further investigated in Fig. 15, which refers to Architecture 1. This figure presents the ECDF of the number of iterations required for UEs' detection relative to Anchor 4 (located at the bottom-left in Fig. 10). The LOS free-space channel is here considered (similar outcomes are achieved with the 3GPP channel model).

A noticeable difference in the number of iterations required for convergence is observed between using a random beamforming vector (blue/red lines) and the last available beamforming vector (yellow/green lines) as initialization of the proposed estimation scheme. The results demonstrate that utilizing the previous beamforming vector yields consistent improvement in terms of the number of iterations needed for convergence. This improvement is particularly significant for U2, which is the farthest from Anchor 4, thus experiencing highly correlated channels from one localization step to the other (as discussed in Section IV-B). Remarkably, when exploiting the previous beamforming vector, the convergence time is halved for $g = 0\,dB$.

These results also offer insights into the localization update rate $\mathcal{R}$. While we set $\mathcal{R} = 10$ Hz in our simulations, much higher values could have been chosen, as the lower limit on this parameter is determined by the packet size K. In fact, the time elapsed between consecutive localization steps must be greater than KT (see Fig. 5), which corresponds to the duration of the ID transmission. Depending on the number of RAAs in the environment, to ensure the discrimination of each ID a certain number of different PN sequences must be available. By assuming, as an example, the adoption of maximum length sequences, a packet length of $K = 1023$ symbols allows discriminating 60 different RAAs, while a packet length of $K = 8191$ symbols allows discriminating 630 different RAAs [13]. These values lead to a maximum localization update rate $\mathcal{R}$ of roughly 10 kHz and 1 kHz, respectively, which is larger than today's RTLSs, that usually provide tens of update per second. In fact, in this case, scalability is much simpler than in time-based RTLSs, where multiple users are usually interrogated sequentially. Since convergence is realized in a few iterations (e.g., 10 is a typical value according to Fig. 15) the detection/estimation time results generally negligible with respect to the ID duration.

In addition to offering a very high localization update rate, the proposed solution offers several advantages over currently available solutions, such as UWB-based RTLSs; in fact, it can work with narrowband transmissions, no synchronization is required as for time-difference-of-arrival based systems, and no clock drift is experienced. Consequently, UWB-based RTLSs results in a more complex anchor localization calibration process compared to our scheme [48]. Moreover, being the RAAs backscattering devices, energy harvesting techniques can be included to make them energy autonomous.

E. Implementation Challenges

Implementing the proposed localization schemes involves addressing some challenges, mostly from the hardware design point of view: *(i)* the interrogating device must operate in full-duplex mode with suitable transmit-receive isolation; *(ii)* to further increase the operating range, the adoption of active RAAs is preferable. As an alternative, the number of antenna elements can be increased to improve the link budget through the beamforming gain. To this end, the exploitation of high-frequency bands might be beneficial to reduce the size; *(iii)* RAA designs must ensure operation with wide angular ranges and provide high symmetry between forward and backward channels. Additional investigations and measurements must address potential risks that come from self-interference with other sources and clutter from other reflectors.

VI. Conclusion

This study introduced two network architectures for localizing mobile devices using backscattering RAAs. An iterative scheme is proposed for these architectures, enabling fast beamforming and AoA estimation without requiring channel estimation. This approach fully leverages MIMO gains, addressing the two-way path loss challenge inherent to backscattering, particularly at mmWave/THz frequencies. As a result, the architectures support simple, cost-effective, and energy-efficient devices, eliminating the need for dedicated signaling or onboard signal processing for RAA-equipped devices. An enhanced version of the scheme is also introduced to track channels for mobile devices, enabling even faster AoA estimation when mobility remains below an analytically-determined speed threshold. Numerical results demonstrate the scheme's effectiveness, achieving centimeter-level localization accuracy with narrowband signals and a limited number of anchors. It also delivers high update rates and ultra-low latency, meeting the stringent requirements of dynamic environments, including vehicular scenarios.

REFERENCES

[1] C. D. Lima et al., "Convergent communication, sensing and localization in 6G systems: An overview of technologies, opportunities and challenges," *IEEE Access*, vol. 9, pp. 26902–26925, 2021.

[2] H. Sarieddeen, N. Saeed, T. Y. Al-Naffouri, and M.-S. Alouini, "Next generation terahertz communications: A rendezvous of sensing, imaging, and localization," *IEEE Commun. Mag.*, vol. 58, no. 5, pp. 69–75, May 2020.

[3] H. Wymeersch, G. Seco-Granados, G. Destino, D. Dardari, and F. Tufvesson, "5G mmWave positioning for vehicular networks," *IEEE Wireless Commun. Mag.*, vol. 24, no. 6, pp. 80–86, Dec. 2017.

[4] S. Bartoletti et al., "Positioning and sensing for vehicular safety applications in 5G and beyond," *IEEE Commun. Mag.*, vol. 59, no. 11, pp. 15–21, Nov. 2021.

[5] R. Whiton, "Cellular localization for autonomous driving: A function pull approach to safety-critical wireless localization," *IEEE Veh. Technol. Mag.*, vol. 17, no. 4, pp. 28–37, Dec. 2022.

[6] M. Säily, O. N. C. Yilmaz, D. S. Michalopoulos, E. Pérez, R. Keating, and J. Schaepperle, "Positioning technology trends and solutions toward 6G," in *Proc. IEEE 32nd Annu. Int. Symp. Pers., Indoor Mobile Radio Commun.*, 2021, pp. 1–7.

[7] S.-W. Ko, H. Chae, K. Han, S. Lee, D.-W. Seo, and K. Huang, "V2X-based vehicular positioning: Opportunities, challenges, and future directions," *IEEE Wireless Commun.*, vol. 28, no. 2, pp. 144–151, Apr. 2021.

[8] N. Decarli, A. Guerra, C. Giovannetti, F. Guidi, and B. M. Masini, "V2X sidelink localization of connected automated vehicles," *IEEE J. Sel. Areas Commun.*, vol. 42, no. 1, pp. 120–133, Jan. 2024.

[9] S. Bartoletti et al., "Integration of sensing and localization in V2X sidelink communications," *IEEE Commun. Mag.*, vol. 62, no. 8, pp. 185–191, Aug. 2024.

[10] A. Guerra, D. Dardari, and P. M. Djuric, "Dynamic radar networks of UAVs: A tutorial overview and tracking performance comparison with terrestrial radar networks," *IEEE Veh. Technol. Mag.*, vol. 15, no. 2, pp. 113–120, Jun. 2020.

[11] M. Ehrig et al., "Reliable wireless communication and positioning enabling mobile control and safety applications in industrial environments," in *Proc. IEEE Int. Conf. Ind. Technol.*, 2017, pp. 1301–1306.

[12] A. Motroni, A. Buffi, and P. Nepa, "A survey on indoor vehicle localization through RFID technology," *IEEE Access*, vol. 9, pp. 17921–17942, 2021.

[13] N. Decarli, F. Guidi, and D. Dardari, "Passive UWB RFID for tag localization: Architectures and design," *IEEE Sensors J.*, vol. 16, no. 5, pp. 1385–1397, Mar. 2016.

[14] S. Zhang, W. Wang, S. Tang, S. Jin, and T. Jiang, "Robot-assisted backscatter localization for IoT applications," *IEEE Trans. Wireless Commun.*, vol. 19, no. 9, pp. 5807–5818, Sep. 2020.

[15] N. Decarli, M. D. Prete, D. Masotti, D. Dardari, and A. Costanzo, "High-accuracy localization of passive tags with multisine excitations," *IEEE Trans. Microw. Theory Tech.*, vol. 66, no. 12, pp. 5894–5908, Dec. 2018.

[16] C. Xu, L. Yang, and P. Zhang, "Practical backscatter communication systems for battery-free Internet of Things: A tutorial and survey of recent research," *IEEE Signal Process. Mag.*, vol. 35, no. 5, pp. 16–27, Sep. 2018.

[17] R. Miesen et al., "Where is the tag?," *IEEE Microw. Mag.*, vol. 12, no. 7, pp. S49–S63, Dec. 2011.

[18] M. El-Absi et al., "High-accuracy indoor localization based on chipless RFID systems at THz band," *IEEE Access*, vol. 6, pp. 54355–54368, 2018.

[19] J. He, A. Fakhreddine, and G. C. Alexandropoulos, "RIS-augmented millimeter-wave MIMO systems for passive drone detection," in *Proc. IEEE 35th Int. Symp. Pers., Indoor Mobile Radio Commun.*, 2024.

[20] A. Pastrav, C. Codau, E. Puschita, P. Dolea, and T. Palade, "Conceptual architecture of a retrodirective antenna system with beamforming capabilities," in *Proc. Int. Conf. Commun.,* 2018, pp. 225–230.

[21] S.-C. Yen and T.-H. Chu, "A retro-directive antenna array with phase conjugation circuit using subharmonically injection-locked self-oscillating mixers," *IEEE Trans. Antennas Propagat.*, vol. 52, no. 1, pp. 154–164, Jan. 2004.

[22] R. Miyamoto and T. Itoh, "Retrodirective arrays for wireless communications," *IEEE Microw. Mag.*, vol. 3, no. 1, pp. 71–79, Mar. 2002.

[23] D. Tagliaferri, M. Mizmizi, G. Oliveri, U. Spagnolini, and A. Massa, "Reconfigurable and static EM skins on vehicles for localization," *IEEE Trans. Wireless Commun.*, vol. 23, no. 11, pp. 16155–16171, Nov. 2024.

[24] N. B. Buchanan, V. F. Fusco, and M. v. d. Vorst, "SATCOM retrodirective array," *IEEE Trans. Microw. Theory Tech.*, vol. 64, no. 5, pp. 1614–1621, May 2016.

[25] Z. Zhu, W. Hu, X. Lin, and X. Li, "A sub-terahertz retrodirective antenna array for satellite tracking," in *Proc. 44th Int. Conf. Infrared, Millimeter, Terahertz Waves*. 2019, pp. 1–2.

[26] S. Karode and V. Fusco, "Self-tracking duplex communication link using integrated retrodirective antennas," in *Proc. IEEE MTT-S Int. Microw. Symp. Dig.*, 1998, vol. 2, pp. 977–980.

[27] E. Soltanaghaei et al., "Millimetro: mmWave retro-reflective tags for accurate, long range localization," in *Proc. 27th Annu. Int. Conf. Mobile Comput. Netw.*, 2021, pp. 69–82.

[28] J. G. Hester and M. M. Tentzeris, "A mm-Wave ultra-long-range energy-autonomous printed RFID-enabled Van-Atta wireless sensor: At the crossroads of 5G and IoT," in *Proc. IEEE MTT-S Int. Microw. Symp.,* 2017, pp. 1557–1560.

[29] S. Gupta and E. Brown, "Noise-correlating radar based on retrodirective antennas," *IEEE Trans. Aerosp. Electron. Syst.*, vol. 43, no. 2, pp. 472–479, Apr. 2007.

[30] Z.-b. Zhu et al., "A high-precision terahertz retrodirective antenna array with navigation signal at a different frequency," *Front. Inf. Technol. Electron. Eng.*, vol. 21, no. 3, pp. 377–383, Apr. 2020.

[31] L. C. V. Atta, "Electromagnetic reflector," U.S. Patent 2,908,002, Oct., 1959.

[32] M. Kalaagi and D. Seetharamdoo, "Fano resonance based multiple angle retrodirective metasuface," in *Proc. 14th Eur. Conf. Antennas Propag.*, 2020, pp. 1–4.

[33] F. Salas, W. Alomar, and A. Grbic, "A phase conjugating metasurface," in *Proc. 14th Int. Congr. Artif. Mater. Novel Wave Phenomena*, 2020, pp. 198–200.

[34] D. Dardari, M. Lotti, N. Decarli, and G. Pasolini, "Establishing multi-user MIMO communications automatically using retrodirective arrays," *IEEE Open J. Commun. Soc.*, vol. 4, pp. 1396–1416, 2023.

[35] D. Dardari, P. Closas, and P. M. Djuric, "Indoor tracking: Theory, methods, and technologies," *IEEE Trans. Veh. Technol.*, vol. 64, no. 4, pp. 1263–1278, Apr. 2015.

[36] C. B. Barneto, S. D. Liyanaarachchi, M. Heino, T. Riihonen, and M. Valkama, "Full duplex radio/radar technology: The enabler for advanced joint communication and sensing," *IEEE Wireless Commun.*, vol. 28, no. 1, pp. 82–88, Feb. 2021.

[37] J.-F. Bousquet, S. Magierowski, and G. G. Messier, "A 4-GHz active scatterer in 130-nm CMOS for phase sweep amplify-and-forward," *IEEE Trans. Circuits Syst. I: Reg. Papers*, vol. 59, no. 3, pp. 529–540, Mar. 2012.

[38] Z. Zhang et al., "Active RIS vs. passive RIS: Which will prevail in 6G?," *IEEE Trans. Wireless Commun.*, vol. 71, no. 3, pp. 1707–1725, Mar. 2023.

[39] C. Allen, K. Leong, and T. Itoh, "A negative reflective/refractive "meta-interface" using a bi-directional phase-conjugating array," in *Proc. IEEE MTT-S Int. Microw. Symp. Dig., 2003*, vol. 3, 2003, pp. 1875–1878.

[40] E. Sharp and M. Diab, "Van Atta reflector array," *IRE Trans. Antennas Propag.*, vol. 8, no. 4, pp. 436–438, Jul. 1960.

[41] N. Decarli, F. Guidi, and D. Dardari, "A novel joint RFID and radar sensor network for passive localization: Design and performance bounds," *IEEE J. Sel. Topics Signal Process.*, vol. 8, no. 1, pp. 80–95, Feb. 2014.

[42] G. H. Golub and H. A. v. d. Vorst, "Eigenvalue computation in the 20th century," *J. Comput. Appl. Math.*, vol. 123, no. 1, pp. 35–65, Oct. 2000. [Online]. Available: https://www.sciencedirect.com/science/article/pii/S0377042700004131

[43] E. Björnson, J. Hoydis, and L. Sanguinetti, "Massive MIMO networks: Spectral, energy, and hardware efficiency," *Found. Trends Signal Process.*, vol. 11, no. 3-4, pp. 154–655, 2017, doi: 10.1561/2000000093.

[44] H. Q. Ngo, E. G. Larsson, and T. L. Marzetta, "Aspects of favorable propagation in massive MIMO," in *Proc. 22nd Eur. Signal Process. Conf.*, 2014, pp. 76–80.

[45] D. Dardari, M. Lotti, N. Decarli, and G. Pasolini, "Grant-free random access with backscattering self-conjugating metasurfaces," *IEEE Trans. Cogn. Commun. Netw.*, vol. 10, no. 5, pp. 1620–1634, Oct. 2024.

[46] A. Pages-Zamora, J. Vidal, and D. Brooks, "Closed-form solution for positioning based on angle of arrival measurements," in *Proc. 13th IEEE Int. Symp. Pers., Indoor Mobile Radio Commun.*, 2002, vol. 4, pp. 1522–1526.

[47] 3GPP, "Study on channel model for frequencies from 0.5 to 100GHz," 3GPP, Tech. Rep. 38.901, 2019.

[48] D. Dardari, A. Conti, U. Ferner, A. Giorgetti, and M. Z. Win, "Ranging with ultrawide bandwidth signals in multipath environments," *Proc. IEEE*, vol. 97, no. 2, pp. 404–426, Feb. 2009.

Marina Lotti (Graduate Student Member, IEEE) received the B.S. and M.S. (cum laude) degrees in electronics and telecommunication engineering from the University of Bologna, Bologna, Italy, in 2017 and 2020, respectively, where she is currently working toward the Ph.D. degree addressing Smart Radio Environments exploiting Reconfigurable Intelligent Surfaces. From 2020 to 2021, she was a Research Engineer with CEA-Leti, France, working on channel characterizations in the subTHz frequency range and radar measurements for localization and mapping purposes.

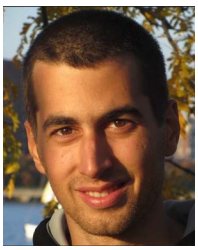

Nicolò Decarli (Member, IEEE) received the Ph.D. degree in electronics, telecommunications, and information technologies from the University of Bologna, Bologna, Italy, in 2013. In 2012, he was a Visiting Student with the Wireless Communication and Network Sciences Laboratory, Massachusetts Institute of Technology, Cambridge, MA, USA. He is currently a Researcher with the Institute of Electronics, Computer, and Telecommunication Engineering, National Research Council of Italy. His research interests include wireless communication theory, integration of communication, localization and sensing, and smart radio environments.

Gianni Pasolini (Member, IEEE) received the M.Sc. degree in telecommunications engineering and the Ph.D. degree in electronic engineering and computer science from the University of Bologna, Bologna, Italy, in 1999 and 2003, respectively. He is currently an Associate Professor with the Department of Electrical, Electronic and Information Engineering, University of Bologna, where he has been teaching various courses in the field of telecommunications since 2003. He is an Associate Editor for the IEEE OPEN JOURNAL OF THE COMMUNICATIONS SOCIETY. His research interests include wireless communication systems, Internet of Things, digital signal processing, and THz communications. He was the recipient of the Best Paper Award at the 2023 IEEE International Conference on Communications. Throughout his career, he has actively participated in several European initiatives focused on wireless communications, including COST actions and Networks of Excellence. He was a member of the Organizing Committee for the 2011 IEEE International Conference on Ultra-Wideband, the 2017 IEEE International Symposium on Wireless Communication Systems, and the 2018 IEEE International Symposium on Personal, Indoor and Mobile Radio Communications. He is one of the founding members of the "National Laboratory of Wireless Communications—Wilab" of the National Inter-University Consortium for Telecommunications in Italy.

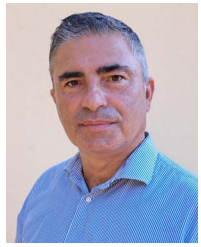

Davide Dardari (Fellow, IEEE) is a Full Professor with the University of Bologna, Bologna, Italy. He has been a Research Affiliate with the Massachusetts Institute of Technology, Cambridge, MA, USA. From 2006 to 2012, he was an Editor for IEEE TRANSACTIONS ON WIRELESS COMMUNICATIONS. He is currently a Senior Member of the Editorial Board of the IEEE Signal Processing Magazine. His research interests include wireless communications, localization techniques, smart radio environments, and distributed signal processing. He was the recipient of the IEEE Aerospace and Electronic Systems Society's M. Barry Carlton Award in 2011 and the IEEE Communications Society Fred W. Ellersick Prize in 2012. He was the Chair of the Radio Communications Committee and a Distinguished Lecturer during 2018-2019 of the IEEE Communications Society.